Variability of the fatigue damage due to the randomness of a stationary vibration load

Julian Marcell Enzveiler Marques, Denis Benasciutti, Roberto Tovo

PII: S0142-1123(20)30422-9
DOI: https://doi.org/10.1016/j.ijfatigue.2020.105891
Reference: JIJF 105891

To appear in: *International Journal of Fatigue*

Received Date: 13 May 2020
Revised Date: 10 August 2020
Accepted Date: 11 August 2020

Please cite this article as: Marcell Enzveiler Marques, J., Benasciutti, D., Tovo, R., Variability of the fatigue damage due to the randomness of a stationary vibration load, *International Journal of Fatigue* (2020), doi: https://doi.org/10.1016/j.ijfatigue.2020.105891

Submitted to International Journal of Fatigue (revised version) – August 2020

Variability of the fatigue damage due to the randomness of a stationary vibration load

Julian Marcell Enzveiler Marques*, Denis Benasciutti, Roberto Tovo

Department of Engineering, University of Ferrara, via Saragat 1, 44122, Ferrara, Italy

ABSTRACT

This paper investigates the variability of the fatigue damage caused by the randomness of a stationary Gaussian random loading. After reviewing some methods from the literature (e.g. Madsen et al., Low), the paper presents a Monte Carlo simulation study to compare such methods with results from time- and frequency-domain analyses. Best-fitting expressions are derived to relate the variability of the damage directly to bandwidth parameters of a PSD. Finally, the paper analyses the variability of the damage when computed from one or few time-histories. For both cases, confidence intervals are constructed to bound the expected damage; simulations confirm their correctness.

Keywords: Random loadings; Fatigue damage; variability of fatigue damage; Coefficient of variation of damage

*Corresponding author. Tel.: +39-0532-974104; fax.: +39-0532-974870

E-mail address: nzvjnm@unife.it

NOMENCLATURE

C_{D}	coefficient of variation of the damage
$\hat{C}_{\mathrm{D}}$	sample coefficient of variation of the damage
d	fatigue damage of a half-cycle
$\overline{D}$	sample mean of fatigue damage
$D(T)$	fatigue damage in time period T
$E[D(T)]$	expected fatigue damage
f	frequency
$f_{P_0,P_l}(x_p,x_v)$	joint probability distribution of peaks and valleys
k, A	material constants of S-N curve
$n(T)$	number of counted half-cycles in T
N	number of time-histories
N_f	number of cycles to failure
$R(\tau)$	autocorrelation function of $X(t)$
$R_{d_0,d_l}(l)$	autocorrelation function of the half-cycle damage
s	stress amplitude of half-cycle
$S(f)$	Power Spectral Density of $X(t)$
T	time length
(x_p,x_v)	peak and valley
$x(t)$	time-history
$X(t)$	random process
$100(1-\beta)$	confidence level

α_1, α_2	bandwidth parameters
ζ	damping
λ_m	m-th order spectral moment
μ_X	mean value of $X(t)$
ν_0	rate of mean value up-crossings
ν_p	rate of peaks
$\rho(\tau)$	autocorrelation coefficient function of $X(t)$
$\rho_{d_0,d_l}(l)$	autocorrelation coefficient function of the half-cycle damage
σ_D^2	sample variance of fatigue damage
$\sigma_D^?$	variance of fatigue damage
$\sigma_X^?$	variance of $X(t)$
τ	time lag

1 INTRODUCTION

Fatigue failures of engineering components and structures may occur as an effect of an applied random loading. Fatigue damage can be estimated in two alternative ways. In a frequency-domain approach, a random process is characterized by a Power Spectral Density (PSD). Mathematical expressions are then used for estimating the expected damage directly from a PSD [1-11]. From a statistical point of view, the expected damage represents the value that would result from averaging all the damage values of an infinite ensemble of time-histories.

By contrast, the time-domain approach computes the damage by processing directly one or more time-histories. It is based on well-established procedures (rainflow counting method and Palmgren-Miner rule), which are probably less complex than the theory behind the frequency-domain approach. Despite this, the time-domain approach usually needs time-histories of a sufficiently long duration to make the computed damage achieve an acceptable small statistical scatter.

Indeed, when in time-domain the damage is computed from only one stationary random time-history $x_1(t)$ of finite length T, it must be regarded as being one sample value out of an infinite population. This value has an intrinsic statistical scatter. In fact, the damage is likely to change if it is computed from another time-history $x_2(t)$, even if this one has exactly the same time length and statistical properties of $x_1(t)$. The two time-histories may, in fact, have different rainflow cycles. And similarly if the damage is computed from a third time-history $x_3(t)$ [9]. This result is explained by the intrinsic randomness of each time-history, which makes the rainflow cycles vary among distinct sample records. Viewed from the theory of random processes, each time-history $x_i(t)$ is conceived of as being one element out of an infinite ensemble; its fatigue damage, in turn, is one value out of an infinite set of damage values [12].

In either way of reasoning, the $D(T)$ damage of $x_i(t)$ of finite length T is a random variable following a certain damage probability distribution. The variance around the expected damage is an essential property of the damage probability distribution – from now on, this will be called the

"variance of the damage". In the structural durability assessment of structures, estimating the variance of the damage becomes as much important as estimating the expected damage [12]. The paper focus is to investigate the variability of the fatigue damage in stationary Gaussian random loadings that comes from the inherent randomness of the loading itself.

In the early sixties, Mark and Crandall [13] have been the first who developed a theoretical approach to assess the variance of the damage. Their method was, however, limited to the linear oscillator system (Gaussian) and to odd integer values of the S-N inverse slope k. A few years later, Bendat [15] contributed with a method applicable to both odd and even integer values of k, even though still restricted to the linear oscillator system. The Bendat's method lies on the assumption that the autocorrelation coefficient function of the half-cycle damage, $\rho_{\mathrm{d}_0,\mathrm{d}_l}(l)$, decays exponentially [15].

Only in the eighties, Madsen et al. [16] devised a more general method for estimating the variance of the damage. Though no more restricted to the linear oscillator, the method applies to Gaussian processes with a narrow-band PSD. To determine the variance, the method requires one to compute the autocorrelation coefficient function of the half-cycle damage, $\rho_{\mathrm{d}_0,\mathrm{d}_l}(l)$, by an approximate relationship relating it to the autocorrelation coefficient function of the random process, $\rho(l)$. It has been only recently that Low proposed a similar approach [17], also valid for narrow-band Gaussian processes, in which the autocorrelation coefficient function $\rho_{\mathrm{d}_0,\mathrm{d}_l}(l)$ is approximated by a best-fitting expression.

This preliminary survey emphasized the fundamental role of the damage autocorrelation coefficient function $\rho_{\mathrm{d}_0,\mathrm{d}_l}(l)$ in all methods but the Mark and Crandall's one. Being it nothing more than a normalized autocorrelation function, the quantity $\rho_{\mathrm{d}_0,\mathrm{d}_l}(l)$ measures how much comparable are, on average, the damage values d_0, d_l of two half-cycles that are l seconds apart. For example, in a narrow-band process (which is highly "correlated", and thus has half-cycles at regularly spaced time intervals and with similar amplitudes) the amplitude of $\rho_{\mathrm{d}_0,\mathrm{d}_l}(l)$ decays rather slowly. By contrast, it

decays faster in a wide-band process that, being less "correlated", has half-cycles with less comparable amplitudes – this point will be addressed in more detail in the article.

All the above-mentioned methods – and the last two, in particular – certainly made the understanding of the complex subject of the variability of the fatigue damage to advance significantly. A small disadvantage of the latter two methods, in a certain sense, is the amount of computation required to determine the damage autocorrelation coefficient function $\rho_{\mathrm{d}_0,\mathrm{d}_l}(l)$. In the following, it will be shown that this quantity follows from the autocorrelation function of the random process, $R(\tau)$, or equivalently from the PSD of the process, of which the autocorrelation $R(\tau)$ is the Fourier transform. This computation would not be necessary by having available a mathematical expression to relate the variance of the fatigue damage directly to some PSD bandwidth parameters. Furthermore, each of the above-mentioned methods is nevertheless applicable to a linear oscillator or, at best, to a narrow-band PSD. Despite the attempt to apply the Low's method to mildly wide-band processes (resulting in only small errors) [17], to date no solution exist to tackle the case of a wide-band process. This goal will be pursued here by deriving a best-fitting expression obtained directly from simulation results. Though not derived by theoretical arguments, this 'data-driven' approach has the advantage of providing a simple expression that is also applicable to wide-band processes, either. To this end, the best-fitting expression will be calibrated on a variety of PSDs varying from narrow-band to wide-band.

Another situation – also addressed in this paper – is that of evaluating the variability of the fatigue damage that is computed from a few time-histories (or even only one) of finite time length T. In this situation, in fact, any of the methods mentioned above cannot be applied, in principle, as they require the knowledge of the exact autocorrelation function or PSD, where "exact" stands for the value averaged from an infinite ensemble of time-histories (which in practice is never available). By contrast, in the situation with only few time-histories, the "exact" autocorrelation or PSD are never known exactly, and they can only be estimated. Nothing can be said about the expected damage of

the whole time-history ensemble constituting the random process. In this situation, confidence interval can be used to bound the expected damage.

Furthermore, the approach based on a direct analysis of time-history realizations has another advantage. In fact, it imposes no restrictions on the specific type of PSD allowed for the random loading, as done by the four methods mentioned above. This makes this approach applicable to a far greater class of random loadings, ranging from narrow-band to wide-band ones.

Motivated by these arguments, this paper aims to investigate the variability of the fatigue damage in stationary Gaussian random process, which is due to the randomness intrinsic to the loading itself. The study makes use of both explicit formulas and numerical simulations. After a short theoretical background on random processes (Section 2) and a review of the main formulas for the damage (Section 3) and its variance (Section 4), the paper surveys the explicit formulas provided by four methods from the literature (Section 5), which are then compared with simulation results (Section 6). Simulations consider a linear oscillator system and an ideal unimodal random process, as well as the JONSWAP and Pierson-Moskowitz power spectral densities. Based on all simulation results, best-fitting expressions are derived to correlate the coefficient of variation of the damage to the bandwidth parameter α_1 (Section 7). The expressions apply to a variety of PSDs ranging from narrow-band to wide-band, provided that the proper best-fitting coefficients are used. The last section (Section 8) addresses a situation for which confidence intervals are constructed to bound the expected damage. The proposed approach turns out to be useful when it is not possible to know the "exact" PSD, that is, when only few time-histories (or even just one) are available. The correctness of proposed approach is checked by a simulation example.

2 PROPERTIES OF RANDOM PROCESSES: THEORETICAL BACKGROUND

Let $X(t),\ -\infty < t < \infty$ be a stationary Gaussian random process. It represents an infinite collection (or ensemble) of time-histories, $x_i(t)$. In the time-domain, process $X(t)$ has autocorrelation function [18]:

$$R(\tau) = E[X(t)X(t+\tau)] \tag{1}$$

in which symbol $E[-]$ is the probabilistic expectation and τ is the time lag. The autocorrelation function can be normalized to the mean value μ_X and variance σ_X^2 of the process to obtain the autocorrelation coefficient function (or normalized autocorrelation function) [19]:

$$\rho(\tau) = \frac{R(\tau) - \mu_X^2}{\sigma_X^2} \tag{2}$$

where $-1 \leq \rho(\tau) \leq 1$. Without loss of generality, it is assumed that $\mu_X = 0$, so that Eq. (2) reduces to $\rho(\tau) = {}^{R(\tau)}/_{\sigma_X^2}$. The random process is also described in the frequency-domain by a one-sided PSD $S(f)$, which is related to the autocorrelation function by a Fourier transform (Wiener-Khinchine relations) [19]:

$$S(f) = 4\int_0^\infty R(\tau)\, cos(2\pi f\tau)\, d\tau \qquad R(\tau) = \int_0^\infty S(f)\, cos(2\pi f\tau)\, df \tag{3}$$

The power spectrum $S(f)$ admits the spectral moments [18]:

$$\lambda_m = \int_0^\infty (2\pi f)^m S(f)\, \mathrm{d}f, \quad m = 0,1,2... \tag{4}$$

where f is the frequency in Hertz. The variance of $X(t)$ is $\sigma_X^2 = \lambda_0$. Spectral moments are also used to compute the average frequency of upward crossings of the mean, $\nu_0 = \sqrt{{\lambda_2}/{\lambda_0}}/2\pi$, and of the peaks, $\nu_p = \sqrt{{\lambda_4}/{\lambda_2}}/2\pi$. The PSD is also characterized by bandwidth parameters; the most used are [18]:

$$\alpha_1 = \frac{\lambda_1}{\sqrt{\lambda_0\lambda_2}}, \qquad \alpha_2 = \frac{\lambda_2}{\sqrt{\lambda_0\lambda_4}} \tag{5}$$

The quantity α_1 is called the groupness parameter in ocean engineering [20,21] and it is related to the definition and properties of the envelope of a random process [22]. The parameter $\alpha_2 = {\nu_0}/{\nu_p}$ is the irregularity factor, defined as the ratio of the number of mean upward crossings to the number of peaks [18]. Both parameters provide a measure of the spectral width of a PSD. They are close to unity

when the process is narrow-band (PSD with a well-defined frequency). Conversely, they tend to zero when the process is wideband (PSD over a larger frequency range) [18].

3 EXPECTED FATIGUE DAMAGE

Let $x(t)$, $0 < t < T$, be a random time-history of time duration T. A counting method (e.g. rainflow) is generally used to identify the fatigue cycles. Cycle counting is especially important in wide-band random loadings to distinguish small cycles that are interruptions of larger ones, but not for narrow-band loadings in which cycle counting is obvious since all cycles are formed by pairing peaks and valleys symmetric with respect to the mean value. The fatigue damage under Palmgren-Miner rule sums up the damage of every half-cycle counted in T:

$$D(T) = \sum_{i=0}^{n(T)-1} d_{\mathrm{i}} = \sum_{i=0}^{n(T)-1} \frac{s_i^k}{2A} \tag{6}$$

in which s_i is the stress amplitude of the i-th half-cycle, $n(T)$ denotes the number of counted half-cycles (reversals), A and k are material constants of the S–N curve $s^k N_f = A$. The fatigue strength constant is usually defined as $A = s_A^k N_{f,A}$ in terms of the fatigue strength amplitude s_A at the reference number of cycles $N_{f,A}$ (typically equal to $2 \cdot 10^6$). The S-N parameters k and A (or s_A) represent the best-fitting estimates of experimental fatigue data. Statistical methods are used to account for both the uncertainty in the estimates and the intrinsic scatter in experimental data. For example, the value of s_A can be calculated for a given survival probability, e.g. 97.7%. [23].

Although it is known that the linearity in Eq. (6) neglects sequential effects in the load (many nonlinear damage accumulation models have indeed been proposed to address this issue [24]), in practical situations the Palmgren-Miner rule remains the most used damage accumulation hypothesis. In its original formulation, fatigue failure occurs when $D(T)$ reaches a critical damage equal to unity, but experimental observations have proved that a more correct value is, on average, close to 0.5 (see for example [25]); this value is also recommended in some design codes for welded joints [26]. Moreover, in the case of spectrum or random loading it also recommended to extrapolate linearly the

S-N curve below the knee point ("endurance limit") [27,28] by adopting a single-slope equation as the one, $s^k N_f = A$, used in the present study.

Damage $D(T)$ strictly depends on the particular set of half-cycles counted in the time-history $x(t)$ of time duration T. Since the number of cycles and their stress amplitudes are randomly distributed, the damage $D(T)$ is a random variable.

The expectation of Eq. (6) gives the expected damage value:

$$E[D(T)] = E\left[\sum_{i=0}^{n(T)-1} d_i\right] = E[n(T)]\frac{E[s^k]}{2A} \tag{7}$$

Eq. (7) represents the limit case in which the damage is computed from the whole ensemble of time-histories, or from an ergodic time-history of infinite time length. The value $E[D(T)]$ thus represents the damage of process $X(t)$. The quantity $E[n(T)]$ is the expected number of half-cycles counted in T, whereas the term $E[d] = E[s^k]/2A$ represents the expected damage per half-cycle. As the rainflow method counts as many cycles as the number of peaks in the time-history, the expected number of half-cycles equals $E[n(T)] = 2\nu_p T$.

For a very narrow-band process, the amplitude distribution coincides with the peak distribution. If the random process is also Gaussian, the amplitudes follow a Rayleigh distribution; the resulting expected damage per half-cycle is [15,29,30]:

$$E[d] = \frac{1}{2A}\left(\sqrt{2\lambda_0}\right)^k \Gamma\left(1+\frac{k}{2}\right) \tag{8}$$

where $\Gamma(-)$ is the gamma function. In a narrow-band process, it is also $\nu_p \cong \nu_0$ and the expected number of half-cycles can be written as $E[n(T)] = 2\nu_0 T$. Using the relationship $E[D(T)] = E[n(T)] \cdot E[d]$, the resulting damage equation for a narrow-band process is [15,29,30]:

$$E[D(T)] = \frac{\nu_0 T}{A}\left(\sqrt{2\lambda_0}\right)^k \Gamma\left(1+\frac{k}{2}\right) \tag{9}$$

This formula is known to be too conservative with a wide-band process and, in this case, other expressions from other methods must be preferred (as for example the TB method) [9].

4 VARIANCE OF FATIGUE DAMAGE IN A NARROW-BAND PROCESS

This section summarizes some general equations of the variance of the fatigue damage in a narrow-band process; they will be further specified by the various methods reviewed in later subsections. Similarly to what done in the preceding Section, also here the notation complies to that adopted in [15,17].

The variance of the fatigue damage is simply the variance of $D(T)$ [15]:

$$\sigma_D^2 = \mathrm{Var}\left[\sum_{i=0}^{n(T)-1} d_i\right] = E\left[\sum_{i=0}^{n(T)-1}\sum_{j=0}^{n(T)-1} d_i d_j\right] - \left(E\left[\sum_{i=0}^{n(T)-1} d_i\right]\right)^2 \tag{10}$$

The second equality follows from the definition of the variance of a random variable $\mathrm{Var}[D(T)] = E\left[D^2(T)\right] - (E[D(T)])^2$. As for the damage, also the variance considers two sources of randomness, namely that of the stress amplitudes and of the number of half-cycles. Due to a small scatter around its mean value, the number of counted cycles $n(T)$ can be assumed to be a deterministic value that, in a narrow-band process, is equal to $n(T) = 2\nu_0 T$. The variance in Eq. (10) is then a direct function of $n(T)$ and an indirect function of T.

Since $n(T)$ is deterministic, both expectations in Eq. (10) can move inside the double and single summation, respectively. Omitting time T, the variance expression then becomes:

$$\sigma_D^2 = \sum_{i=0}^{n-1}\sum_{j=0}^{n-1} E[d_i d_j] - \left(\sum_{i=0}^{n-1} E[d_i]\right)^2 \tag{11}$$

The double summation in Eq. (11) can be interpreted as the aggregate of the elements in a $n \times n$ matrix, as represented in Figure 1.

Since the process $X(t)$ is stationary, the half-cycle damage process d_i is stationary, too. This implies that the sum of all elements in the main diagonal (see Figure 1) yields the term $nE\left[d_0^2\right]$ and the sum of off-diagonal terms corresponds to $(n-l)E[d_0 d_l]$, where $l = j - i$ takes on integer values from 1 to $n-1$. As the elements in any diagonal are identical, the double summation then reduces to a single summation.

On the hypothesis that the half-cycle damage is stationary, the expectation $E[d_i]$ in Eq. (11) implies that $E[d_0] = E[d_1] = ... = E[d_{n-1}]$, from which the single summation squared results into n^2 $E[d_0]^2$. The variance of the fatigue damage in Eq. (11) can thus be rewritten as [17]:

$$\sigma_D^2 = n\left(E[d_0^2] - E[d_0]^2\right) + 2\sum_{l=1}^{n-1}(n-l)\left(E[d_0 d_l] - E[d_0]^2\right) \tag{12}$$

The expected cross-product defines the autocorrelation function of the half-cycle damage, $R_{d_0,d_l}(l)$ $= E[d_0 d_l]$. The term $E[d_0^2]$ is the value at zero time lag, $E[d_0^2] = R_{d_0,d_l}(0)$. The difference between $R_{d_0,d_l}(0)$ and the mean squared $E[d_0]^2 = \mu_d^2$ provides the variance of the half-cycle damage, $R_{d_0,d_l}(0)$ $- \mu_d^2 = \sigma_d^2$.

In analogy with the random process $X(t)$, an autocorrelation coefficient function of the half-cycle damage is introduced as:

$$\rho_{d_0,d_l}(l) = \frac{R_{d_0,d_l}(l) - \mu_d^2}{\sigma_d^2} \tag{13}$$

which is bounded as $0 \leq \rho_{d_0,d_l}(l) \leq 1$. The parameter $\rho_{d_0,d_l}(l)$ measures the correlation between the random variables d_0 and d_l drawn from the same random process.

Under the hypothesis of deterministic number of half-cycles, Eq. (12) represents the expression of the variance of the damage for a stationary narrow-band random process. The expression can also be written as a function of $\rho_{d_0,d_l}(l)$ [17]:

$$\sigma_D^2 = \left[n + 2\sum_{l=1}^{n-1}(n-l)\rho_{d_0,d_l}(l)\right]\left(E[d_0^2] - E[d_0]^2\right) \tag{14}$$

This equation makes apparent the fundamental role of the autocorrelation coefficient function $\rho_{d_0,d_l}(l)$ in the computation of the variance of the damage. The four methods reviewed in the next Section on differ on the basis of which expression is assumed for the autocorrelation coefficient function. In turn, the quantity $\rho_{d_0,d_l}(l)$ depends on the damage autocorrelation function $R_{d_0,d_l}(l) = E[d_0 d_l]$ through Eq. (13).

Now consider two peaks, P_0 and P_l, separated by a time difference $\tau = {}^{l}/_{(2\nu_0)}$. Like in [17], throughout the text the term ‘‘peak’’ is used in a broad sense to mean also valley. It should be noted that, in a narrow-band process, the stress amplitude is equal to the peak value, $s_l = P_l$. Therefore, the damage per half-cycle d_l is proportional to P_l^k. Accordingly, the product $E[d_0 d_l]$ can be computed from the joint probability density function (JPDF) of two peaks, $f_{P_0,P_l}(x_p,x_v)$ as:

$$E[d_0 d_l] = \frac{1}{4A^2}\iint_{-\infty}^{\infty} x_p^k x_v^k \, f_{P_0,P_l}(x_p,x_v)\mathrm{d}x_p\mathrm{d}x_v \tag{15}$$

This equation makes apparent that $E[d_0 d_l]$ depends upon the JPDF $f_{P_0,P_l}(x_p,x_v)$, which thus plays an important role when computing the variance of the damage. For example, the Low’s method considers the Rice’s formula valid for a narrow-band process [17].

5 REVIEW OF EXISTING METHODS

5.1 Mark and Crandall’s method (1961)

Mark and Crandall proposed the first explicit formula to estimate the variance of the fatigue damage [13,14]. Their method assumes that stress time-histories are proportional to the response of a light damped linear oscillator system. For this special case, which is a narrow-band Gaussian process, Mark and Crandall arrived at the approximated expression for the variance:

$$\sigma_D^2 = \frac{f(k)\nu_0 T}{\zeta A^2}(2\lambda_0)^k \, \Gamma^2\left(1+\frac{k}{2}\right) \qquad \text{for } \zeta \le 0.05 \text{ and } \zeta\nu_0 T \gg 1 \tag{16}$$

where $f(k)$ is a function of odd k and ζ is the damping coefficient of linear oscillator system. The complete analysis leading to $f(k)$ is too long to be reproduced here. The function $f(k)$ has been pre-computed up to $k = 15$; some values are $f(1) = 0.041$, $f(3) = 0.369$, $f(5) = 1.28$, $f(7) = 3.72$ [13,14]. Note that the function $f(k)$ is nonlinear with k. On the other hand, the variance in Eq. (16) increases linearly with $\nu_0 T$ following the same trend as the expected damage in Eq. (9). The variance

of the damage also increases with k or if the damping coefficient ζ turns smaller. The quantity $C = \sigma_D/E[D(T)]$, equal to the ratio of the standard deviation σ_D to the expected value $E[D(T)]$, represents the definition of the coefficient of variation (CoV) of the damage. After substituting the formulas in Eq. (9) and (16) one gets the expression for the Mark and Crandall's method:

$$C_D^{\mathrm{Mar}} = \sqrt{\frac{f(k)}{\zeta \nu_0 T}} \qquad \text{for } \zeta \leq 0.05 \text{ and } \zeta \nu_0 T \gg 1 \tag{17}$$

While the expected value $E[D(T)]$ in Eq. (9) and the variance of the damage in Eq. (16) both increase linearly with $\nu_0 T$, the CoV (which considers the square root of the variance) results to be inversely proportional to $\sqrt{\nu_0 T}$ in the range where Eq. (17) is valid [13].

5.2 Bendat's method (1964)

Bendat developed a more general expression for the variance of the fatigue damage that also applies the linear oscillator system [15]. As an alternative to solving the product $E[d_0 d_l]$ by Eq. (15), Bendat assumed that the autocorrelation coefficient function of the half-cycle damage decays exponentially as $\rho_{d_0,d_l}(l) = \exp(-2l\pi\zeta)$. With this simplification and after substituting Eq. (8) into Eq. (14), the variance of the damage turns into:

$$\sigma_D^2 = \frac{\nu_0 T}{\zeta A^2} (2\lambda_0)^k \left[\Gamma(1+k) - \Gamma^2\left(1 + \frac{k}{2}\right) \right] \tag{18}$$

Compared to Mark and Crandall's approach, now the variance no longer depends on $f(k)$. The corresponding expression of the CoV is:

$$C_D^{\mathrm{Ben}} = \sqrt{\frac{1}{\zeta \nu_0 T} \left[\frac{\Gamma(1+k)}{\Gamma^2\left(1 + \frac{k}{2}\right)} - 1 \right]} \tag{19}$$

Equations (18) and (19) hold for both even and odd integer values of k. Likewise the Mark and Crandall's solution, also the Bendat's equation of the variance is proportional to $\nu_0 T$, whereas that of the CoV is inversely proportional to $\sqrt{\zeta \nu_0 T}$.

5.3 Madsen et al.'s method (1986)

Madsen et al. proposed a method for any integer value of k and any narrow-band process [16]. The method takes into account the envelope process [31], which matches the peaks of a narrow-band process. Using this envelope, the method computes the parameter $\rho_{d_0,d_l}(l)$ in the form of the expectation of even powers of correlated normal variables, whose result is known from Ref. [32]:

$$\rho_{d_0,d_l}(l) = \frac{1}{2}\left[\rho_l^2 + 2\left(\frac{\rho_l'}{2\pi\nu_0}\right)^2 + \frac{(\rho_l'')^2}{(2\pi\nu_0)^4}\right] \tag{20}$$

in which $\rho_l = \rho(l)$ is the autocorrelation coefficient function computed at lag l, while ρ_l' and ρ_l'' are the first and second derivative of ρ_l with respect to l. After the assumption that $\rho_l'' = -(2\pi\nu_0)^2\rho_l$, Madsen et al. arrived at [16]:

$$\rho_{d_0,d_l}(l) = \rho_l^2 + \left(\frac{\rho_l'}{2\pi\nu_0}\right)^2 \tag{21}$$

By inserting Eq. (21) and Eq. (8) into Eq. (14), the variance is computed as:

$$\sigma_D^2 = \frac{n + 2\sum_{l=1}^{n-1}(n-l)\left[\rho_l^2 + \left(\frac{\rho_l'}{2\pi\nu_0}\right)^2\right]}{4A^2}(2\lambda_0)^k\left[\Gamma(1+k) - \Gamma^2\left(1+\frac{k}{2}\right)\right] \tag{22}$$

Eq. (22) involves a summation of terms related to the autocorrelation coefficient function ρ_l. Note how the variance of the damage derived by Madsen et al. needs not to compute the product $E[d_0 d_l]$. The corresponding CoV is:

$$C_D^{\text{Mad}} = \sqrt{\frac{n + 2\sum_{l=1}^{n-1}(n-l)\left[\rho_l^2 + \left(\frac{\rho_l'}{2\pi\nu_0}\right)^2\right]}{n^2}\left[\frac{\Gamma(1+k)}{\Gamma^2\left(1+\frac{k}{2}\right)} - 1\right]} \tag{23}$$

Also Eq. (23) is a function of the autocorrelation coefficient function ρ_l. Being it valid for any narrow-band process (and not only for a linear oscillator system), the Madsen et al.'s expressions do not depend on the damping coefficient ζ.

Furthermore, this method also holds for non-integer k. In this case, the variance and CoV become function of an hypergeometric function ${}_2F_1\left[-k/2,-k/2;1;\rho^2_{d_0,d_l}(l)\right]$; their expressions can be found in [16].

5.4 Low's method (2012)

This method arrived at a best-fitting expression of $\rho_{d_0,d_l}(l)$ by solving the product expectation in Eq. (15) through the use of the Rice JPDF of peaks and valleys in a narrow-band process [33]:

$$f_{P_0,P_l}(x_p,x_v) = \frac{x_p x_v}{1-\rho_l^2} I_0\left(\frac{x_p x_v\,\rho_l}{1-\rho_l^2}\right)\exp\left(\frac{x_p^2+x_v^2}{-2\left(1-\rho_l^2\right)}\right) \tag{24}$$

where $I_0(-)$ is the modified Bessel function of the first kind with order zero. After substituting this $f_{P_0,P_l}(x_p,x_v)$ into Eq. (15), the resulting double integral has been solved for even values $k = 2, 4, 6$ with the aid of symbolic computation software [17]. Subsequently, in order to include also the odd value of k, the autocorrelation coefficient function $\rho_{\mathrm{d_0,d_l}}$ has been very accurately approximated by a quadratic interpolation function of ρ_l^2 as [17]:

$$\rho_{d_0,d_l} = \alpha_k \rho_l^2 + \beta_k \rho_l^4 \tag{25}$$

where the fitting coefficients α_k and β_k depend upon k (their values are tabulated in [17]). The fitting covered the integer values in the range $1 \le k \le 9$. A linear interpolation is suggested to accommodate non-integer values [17].

With this approximation and by invoking Eq. (8), the variance of the fatigue damage in Eq. (14) results in the form:

$$\sigma_D^2 = \frac{n + 2\sum_{l=1}^{n-1}(n-l)\left(\alpha_k \rho_l^2 + \beta_k \rho_l^4\right)}{4A^2}(2\lambda_0)^k\left[\Gamma(1+k) - \Gamma^2\left(1+\frac{k}{2}\right)\right] \tag{26}$$

Accordingly, the CoV can be written as:

$$C_D^{\text{Low}} = \sqrt{\frac{n + 2\sum_{l=1}^{n-1}(n-l)\left(\alpha_k \rho_l^2 + \beta_k \rho_l^4\right)}{n^2}\left[\frac{\Gamma(1+k)}{\Gamma^2\left(1+\frac{k}{2}\right)} - 1\right]} \tag{27}$$

Note the similarity in the expressions of the CoV given by the methods of Madsen et al. and Low, compare Eq. (23) and (27).

5.5 Critical analysis of the existing methods

The main difference among the previous methods lies in which specific process is considered (linear oscillator or any narrow-band process) and in the way by which the autocorrelation coefficient function of damage $\rho_{d_0,d_l}(l)$ is computed. To this regard, another hypothesis relies on which values are allowed for the S-N inverse slope (i.e. even and/or odd integers, or also non-integers).

Mark and Crandall's pioneering work seems to have the most restrictive hypotheses (light damped oscillator and odd k), which make its application not very general. Bendat's method has the same assumptions of Mark and Crandall's approach, the main difference being that it allows for both odd and even values of k and that it does not impose restrictions to the damping ζ. Also the assumption of an autocorrelation $\rho_{d_0,d_l}(l)$ decaying exponentially seems to be empirical.

By contrast, the method of Madsen et al. and that of Low are far more general. They apply to any narrow-band process (i.e. not only to the linear oscillator), provided that its autocorrelation coefficient function $\rho_l = \rho(l)$ is known. The only difference is how this coefficient enters into the expressions of the variance and CoV, compare Eq. (22)-(23) to Eq. (26)-(27). Basically, this difference follows from the relationship between the autocorrelation coefficient function of the

process, $\rho_l = \rho(l)$, and that of the damage, $\rho_{d_0,d_l}(l)$, which is established by each of the two methods via Eq. (21) or (25).

Among the two, Madsen et al.'s method nevertheless seems to be the most general, since it has no restriction on the allowable values of k. For this reason, it will be used as a reference in the simulation study of Section 6.

One possible limitation of each of the two latter methods is that they ask for the autocorrelation coefficient function of the process, $\rho_l = \rho(l)$, in order to compute the CoV in Eq. (23) and (27), where $\rho(l)$ depends on $R(\tau)$ as in Eq. (2). If $R(\tau)$ is not readily available, it can be determined directly from the PSD after a Fourier transform computation. It would clearly be much easier to by-pass this Fourier transform by relating the CoV directly to PSD bandwidth parameters (e.g. α_1 and α_2). This approach would also allow one to check, with no much effort, whether the above methods are applicable to wide band processes, and up to which spectral width one gets reasonable estimates. This point will be investigated in the next section.

It seems finally not superfluous to highlight that all the above-mentioned four methods are restricted to random loadings that are Gaussian and narrow-band. A solution, not considered here, valid for random loadings with multiple frequency modes was proposed in [34]. Recently, an approach was developed to extend two of the methods (Low, Madsen et al.) to the non-Gaussian case [35].

6 COMPARISON OF EXISTING METHODS: NUMERICAL SIMULATIONS

This section explores the correctness of the explicit formulas provided by the previous methods through the use of Monte Carlo simulations in time- and frequency-domain. Two types of power spectrum $S(f)$ are considered: linear oscillator response, ideal unimodal (rectangular shape). Both are centered at 10 Hz and normalized to $\lambda_0 = 1$, see Figure 2(a) and (b). Other two power spectra

(Pierson-Moskowitz and JONSWAP) are analyzed in Section 6.3 when it comes to find a best-fitting expression to link the CoV to bandwidth parameters.

A total of $N = 2 \cdot 10^5$ stationary Gaussian random time-histories $x_i(t)$, $i = 1,2,3,...N$ with time length T are simulated from each spectrum $S(f)$. Note that the total number of simulated time-histories is comparable or larger than that used in other similar studies [17,34,36]. The digitalized time-histories are generated by the Discrete Fourier Transform approach, which uses deterministic spectral amplitudes and uniformly distributed random phases [37,38]. Three different values of T are selected so that the simulated time-histories have approximately 10^3, 10^4 and 10^5 counted cycles.

An estimated power spectral density $\hat{S}_i(f)$ is also evaluated from each simulated time-history $x_i(t)$ by means of the Welch's windowed overlapped segment averaging technique [19,38]. A Hanning window was selected to mitigate the side-lobe leakage; a 75% overlapping allowed a total of 97 segments for which the statistical error of the spectrum estimate is $\varepsilon_r = 1/\sqrt{97} = 0.10$. For each of the three selected values of T, the analysis provides $N = 2 \cdot 10^5$ estimated power spectra $\hat{S}_i(f)$, one for each simulated time-history.

For every time-history $x_i(t)$, the fatigue damage $D_i(T)$ is finally calculated in both the time-domain and the frequency-domain. The time-domain damage is computed from $x_i(t)$ by using the rainflow counting algorithm and the Palmgren-Miner rule. The frequency-domain damage is computed by Eq. (9) from the estimated power spectrum $\hat{S}_i(f)$. To this regard, this frequency-domain damage should be interpreted as a sample estimate of the expected damage $E[D(T)]$ that is obtained when Eq. (9) is applied to $S(f)$.

It has to be pointed out that each estimated power spectrum $\hat{S}_i(f)$ is characterized by an inherent sampling variability that comes from the fact that the spectrum is evaluated from one single time-history of finite duration [19,38]. This sampling variability makes every estimation $\hat{S}_i(f)$ not exactly equal to the "true" power spectral density $S(f)$ – indeed, the spectral values $\hat{S}_i(f)$ are random variables following a chi-square probability distribution [19,38]. The sampling variability in power

spectrum estimate transfers to the frequency-domain damage and it sums to the variability caused by the randomness of time-history realizations, which instead is the only source of variability included in the time-domain damage.

In all case studies examined, the damage calculation assumes an S-N curve with $A = 1$ and an inverse slope k taking on integer values from 2 to 9. The sample mean damage $\overline{D}(T) = N^{-1} \sum_{i=1}^{N} D_i(T)$, sample variance $\hat{\sigma}_D^2 = (N-1)^{-1} \sum_{i=1}^{N} [D_i(T) - \overline{D}(T)]^2$ and sample CoV $\hat{C}_D = \hat{\sigma}_D / \overline{D}(T)$ are estimated from the set of damage values in time- and frequency-domain. Instead, the expected damage $E[D(T)]$ is calculated by Eq. (9) from the power spectrum $S(f)$.

6.1 Linear oscillator system

The linear oscillator system is here chosen as it allows the explicit formulas provided by all the previous methods to be applied. The system has a light damping that was varied in the values $\zeta =$ 0.005, 0.01, 0.02, 0.05, 0.1, and it is subjected to a band-limited random base acceleration $Z(t)$ with frequency content from 0 to 20 Hz. Analytical expressions are derived for the mass absolute displacement, $Y(t)$, and the relative displacement, $X(t) = Y(t) - Z(t)$. The relative displacement response spectrum $S(f)$ is centered around the natural frequency (see Figure 2(a)) and it is a narrow-band Gaussian process $X(t)$, with bandwidth parameters ranging from $\alpha_1 = 0.998$, $\alpha_2 = 0.994$ (for $\zeta = 0.005$) to $\alpha_1 = 0.961$, $\alpha_2 = 0.895$ (for $\zeta = 0.1$).

Figure 3(a) displays the trend of the sample mean and the sample standard deviation of the fatigue damage (both normalized to the expected damage) for both time- and frequency-domain results, as a function of the number of counted cycles. The figure refers to the inverse slope $k = 3$ and damping $\zeta =$ 0.005, but similar trends are obtained for other values (a higher damping only decreases the variance values). The box on the left side compares the observed probability distributions corresponding to the three different number of cycles examined. The distributions permit one to appreciate the increase of the standard deviation as the number of cycles diminishes. The

highest (normalized) standard deviation (i.e. the CoV) is due to the unfavorable combination of a low number of cycles and a low damping ζ, as predicted by Eq. (17). It also emphasizes how large is the variability of the damage in time-histories of short length (that is, those with a small number of counted cycles). Figure 3(a) also shows that the greater is the number of counted cycles, the lower is the dispersion around the mean of the damage distribution. For any number of counted cycles, the standard deviation in the frequency-domain seems to be slightly lower (about 1%) than that in the time-domain. In addition, the mean damage in the frequency-domain seems closer to the expected damage. This result seems to confirm that the PSD estimation does not introduce a significant error in the frequency-domain damage.

The trend in Figure 3(a) is further clarified in Figure 3(b), which shows the change of the CoV versus the number of counted cycles. The comparison of the CoV from simulations and all methods shows a good agreement all over the values of counted cycles. The straight lines on a log-log scale have somehow to be expected, as the CoV from any method is inversely proportional to the square root of the number of counted cycles, $\sqrt{\nu_0 T}$.

6.2 Ideal unimodal process

This case study refers to an idealized rectangular spectrum, see Figure 2(b). The effect of the bandwidth (from narrow-band to wide-band process) is incorporated in the half spectral width b, which takes on integer values in the interval from 1 to 10 Hz. Figure 2(b) displays the PSD for these two limit values of b. By increasing b, the bandwidth parameters decrease from $\alpha_1 = 0.998$ and $\alpha_2 = 0.993$ (most narrow-band case) to $\alpha_1 = 0.866$ and $\alpha_2 = 0.745$ (lowest values for the most wide-band case). The CoV from Monte Carlo simulations in the time-domain is compared with the Madsen et al.'s method over the above range of bandwidth parameters. Contrary to the example with the linear oscillator, not all the methods can be applied to the unimodal PSD. Indeed, the ideal unimodal PSD – even if narrow-band – falls outside the range of applicability of both Mark and Crandall's and

Bendat's methods, whereas it is valid for the other two methods of Madsen et al. and Low. On the other hand, these methods are somehow equivalent in that they provide almost coincident results, as shown for example in Figure 3(b), although as already emphasized the Madsen et al.'s method provides the most general expressions for variance and CoV. For this reason, only the Madsen et al.'s method will be included in the figures.

As a first result, Figure 4 displays the autocorrelation coefficient function of the process, $\rho(l)$, and of the half-cycles damage, ρ_{d_0,d_l}, and compares them for the two limit spectral bandwidths corresponding to the most narrow-band and most wide-band process. The figure allows one to grasp immediately the different behavior of ρ_{d_0,d_l}: its amplitude decays faster in a wide-band process than in a narrow-band one. In the former case, the process is less "correlated" and thus even adjacent half-cycles do not have similar values of their amplitude and, in turn, of their damage – on average, the product $R_{d_0,d_l}(l) = E[d_0 d_l]$ in the definition of ρ_{d_0,d_l} is close to zero even for small l.

Figure 5(a) displays, for $k = 3$, a typical trend of the CoV over the number of counted cycles, for two limit cases $b = 1$ Hz and $b = 10$ Hz (the curves for other intermediate cases are not shown to avoid clutter). Other k values lead to identical trends.

For a narrow-band process ($\alpha_1 = 0.998$, $\alpha_2 = 0.993$), Madsen et al.'s method overlaps results of time-domain simulations. Once the ideal unimodal tends to the limit wide-band case ($\alpha_1 = 0.866$, $\alpha_2 = 0.745$), the CoV decreases. Despite Madsen et al.'s method only applies to the narrow-band case, it agrees fairly well (difference of about 25%) with the time-domain results for the wide-band case, too.

It is also of interest to investigate the relationship (see Figure 5(b)) that links the CoV directly to the bandwidth parameters α_1 and α_2. Figure 5(b) considers two combinations of inverse slope and number of cycles ($k = 3$ and 10^3; $k = 5$ and 10^4); similar trends are obtained for other combinations. The two bandwidth parameters, as already stated in Sec. 2, represent important physical properties of the random process: α_1 provides a unitless measure of the frequency distribution of the PSD of the

process (and it controls some properties of the envelope of the process), whereas α_2 coincides with the irregularity factor of a Gaussian process. Not only are such bandwidth parameters used to classify a PSD type from narrow-band to wide-band, but they often enter the expressions used for estimating the expected damage directly from a PSD (for example, the correction factor λ_{TB} in TB method is a function of α_1 and α_2, see [39]).

Figure 5(b) shows that the CoV increases with α_1 and α_2 (from wide-band to narrow-band process). If k and n are changed, the two trend lines shift upward or downward, while remaining almost unaltered.

6.3 Pierson-Moskowitz (P-M) and JONSWAP and power spectra

The results in Figure 5 suggests that similar tendencies could also characterize other power spectral densities. It was then decided to carry out additional simulations with the two PSDs considered in this Section. Such power spectra are often encountered in offshore engineering and are selected here for illustrative purposes; their equations are reported in Appendix A. Note that the two PSDs here analyzed, being not strictly narrow-band, are outside the range of applicability of the methods reviewed in Section 5, which therefore will not be applied for comparison purposes. The parameters defining both power spectra were assigned so to let the corresponding bandwidth parameters α_1 and α_2 vary over a wide range. The inverse slope varied from 2 to 9, as before.

For the two power spectra in this Section it is certainly of more interest to look at the relationship of CoV to parameter α_1 (see Figure 6), rather than scrutinizing the relationship between CoV and the number of cycles, which in fact follows a trend identical to that of other PSDs (see for example Figure 5(a)). For comparison purposes, Figure 6 plots the curves of all the four spectra examined so far. A common trend stands out clearly. Interestingly, when α_1 approaches unity, the linear oscillator has the higher values of CoV compared to the unimodal PSD with same α_1. In the

region of lower α_1, the JONSWAP power spectrum is characterized by larger values of CoV. Instead, the ideal unimodal PSD always returns the lowest CoV.

7 EMPIRICAL EXPRESSIONS TO RELATE THE COV TO BANDWIDTH PARAMETERS

Figure 6 suggests that a common relationship exists between the CoV of the damage and the bandwidth parameter α_1. Furthermore, the curves in Figure 6 are not only increasing but – more importantly – also smooth. This attribute is advantageous to represent the curves by a best-fitting expression. This expression should be as simple as possible to allow a straightforward evaluation of the CoV.

Based on the previous insights, it is reasonable to assume that the CoV be a function of α_1, k and $\nu_p T$ in the general form $C_D^{\text{fit}} = B(\alpha_1,k) \cdot (\nu_p T)^{-1/2}$. The constant of proportionality $B(\alpha_1,k)$ only depends on α_1 and k. The quantity $\nu_p T = N_p$ is the number of counted cycles in time T, which indeed equals the number of peaks. Using ν_p instead of ν_0 to count the number of half-cycles makes the formula applicable to wide-band processes, either. In the narrow-band case obviously $\nu_0 \cong \nu_p$.

Cast this way, the C_D^{fit} has the desirable property to approach zero for large T, and also to depend on four spectral moments λ_0, λ_1, λ_2, λ_4 through α_1 and ν_p, similarly to the TB method [39].

The trends in Figure 6 suggest that, for k and $\nu_p T$ fixed, the function C_D^{fit} has to be monotonic and satisfy the constraint $C_D^{\text{fit}} \to \infty$ when $\alpha_1 \to 1$. At the same time, when α_1 decreases the function seems to approach a limit value that changes with k and $\nu_p T$, see Figure 5 for the unimodal PSD. Among the mathematical expressions, a rationale polynomial seems to be a possible candidate:

$$C_D^{\text{fit}} = \frac{c_1 \exp\left(k^{c_2}\right)}{\left(1-{\alpha_1}^{c_3}\right)^{c_4}} (\nu_p T)^{-1/2} \tag{28}$$

where c_1, c_2, c_3 and c_4 are unknown fitting coefficients, determined by minimizing the root-mean-square error between the proposed fitting expression, C_D^{fit} and the time-domain simulations, $\hat{C}_D$:

$$e = \sqrt{\frac{1}{q}\sum_{i=1}^{q}\left(C_{D,i}^{\text{fit}} - \hat{C}_{D,i}\right)^2} \tag{29}$$

The sum spans over the q combinations that result from all the considered values of α_1 and the inverse slope in the range $2 \leq k \leq 9$.

At first glance, it seems rather hard to use a single curve to describe the trends in Figure 6 with a satisfactory degree of accuracy. For this reason, the coefficients c_i were calibrated for each PSD separately, see Table 1. As an example, for the unimodal PSD the final expression is:

$$C_D^{\text{fit}} = \frac{0.241\,\exp\left(k^{0.583}\right)}{\left(1-{\alpha_1}^{19.4}\right)^{0.253}}\left(\nu_{\text{p}}T\right)^{-1/2}, \qquad \text{for } 2 \leq k \leq 9 \text{ and } 0.866 \leq \alpha_1 \leq 1 \tag{30}$$

The equation has no restrictions in the values of $\nu_p T$. Figure 7 confirms that the proposed formula agrees very well with the time-domain results, for a range of combinations of k and α_1 of practical interest – the figure refers to 10^3 cycles, but similar results are obtained for other values. In particular, the formula encompasses processes from narrow-band to mildly wide-band.

A similar agreement was obtained for all the other PSDs, as confirmed by the similar fitting errors in the rightmost column of Table 1. Despite the data in Figure 6 are not perfectly overlapped, an attempt was also made to find out a single trend line, by calibrating Eq. (28) on all the data merged together. The coefficients are listed in the last row of Table 1. As expected, a larger error is obtained.

Nevertheless, the decisive advantage of using Eq. (28) lies in the fact that it does not require computing the autocorrelation coefficient function ρ_l, which makes its practical use much easier than using the formula provided by the methods from the literature.

It must, however, be emphasized that the relationship between CoV and α_1 in Eq. (28) is merely empirical. In fact, it has been suggested by the observation of numerical results, rather than it being the outcome of theoretical arguments. Therefore, Eq. (30) does not compromise the validity of the theoretical solutions reviewed in the previous sections, but rather it is complementary to them.

8 ESTIMATION OF THE DAMAGE VARIABILITY WITH FEW TIME-HISTORIES

The explicit formulas discussed so far estimate the variance of the damage directly from the autocorrelation coefficient function ρ_l computed from the power spectrum $S(f)$ – more precisely, ρ_l is linked to the autocorrelation function $R(\tau)$ that, in turn, is computed from $S(f)$ via the inverse Fourier transform in Eq. (3).

However, the exact mathematical formula of the power spectrum $S(f)$ is available only in few cases. Examples are the spectrum of the road profile and that of wind or wave loadings [40,41,42]; they can be input in a structural analysis to get the output stress power spectral density. A fortunate case is the Wirsching's formula that directly provides the approximate output stress power spectrum for an offshore platform [43].

Apart from these exceptions, in most engineering cases the power spectral density must be estimated from time-histories realizations of finite-length, whose number is often very limited. When estimated this way, either the PSD or the autocorrelation function represent sample estimates that are affected by a statistical uncertainty. Some theoretical results are provided in [19] to quantify the variance of the estimated autocorrelation, or the sampling distribution of the estimated spectrum.

Less certain is, however, the knowledge of how this uncertainty propagates to the variance and CoV of the damage computed by the previous four methods. For this reason, an alternative approach is here proposed that, without the need to evaluate the PSD or the autocorrelation function, allows estimating the uncertainty of the fatigue damage in the case in which the damage itself is computed from only one or few time-history realizations. The approach will provide a confidence interval to enclose the expected damage $E[D(T)]$. A further advantage of this approach, if compared to the four methods discussed in the previous Sections, is that it does not require the random process to have any specific type of PSD, which can thus be either narrow-band or wide-band.

From now on, let us assume that the random time-history $x(t)$ of length T is stationary, Gaussian and ergodic. Also, let us assume that its fatigue damage $D(T)$ tends toward the normal distribution [13], with expected value $E[D(T)]$ and variance σ_D^2.

8.1 Confidence interval of the fatigue damage with one single or more time-histories

This subsection will obtain the confidence interval for two distinct cases, depending on the number of time-histories available (see Figure 8): "Case 1" refers to two or more time-histories $x_i(t)$, $i = 1,2,...N$ $(N \geq 2)$ of same duration T, "Case 2" refers to only one time-history $(N = 1)$ with the same duration T as in Case 1. Symbol $D_i(T)$, $i = 1,2,...N$ identifies the fatigue damage of each time-history, computed in the time-domain (rainflow counting and Palmgren-Miner rule). The approach proposed for Case 1 is especially suitable for a small sample size N, as it generally occurs in practice.

Case 1 is discussed first. Assume that N time-histories $x_i(t)$ are available, see Figure 8(a). The sample mean $\overline{D}(T)$ and the sample variance $\hat{\sigma}_D^2$ of the damage are first computed from the set of N damage values $D_i(T)$. These two sample values are the estimates of the exact (but unknown) quantities $E[D(T)]$ and σ_D^2. Following the definition of confidence interval of a normally distributed random variable with unknown mean and unknown variance, the $100(1-\beta)\%$ confidence interval for the expected damage is defined as [44]:

$$\overline{D}(T) - \frac{t_{dof,\beta/2} \cdot \hat{\sigma}_D}{\sqrt{N}} \leq E[D(T)] \leq \overline{D}(T) + \frac{t_{dof,\beta/2} \cdot \hat{\sigma}_D}{\sqrt{N}} \tag{31}$$

where $t_{dof,\beta/2}$ is the quantile of the Student's t-distribution with $dof = N - 1$ degrees of freedom. Equation (31) exploits the fact that $t_{dof,1-\beta/2} = -t_{dof,\beta/2}$. As an example, for $dof = 9$ and $100(1-\beta)\% = 95\%$, it is $t_{9,0.025} = 2.262$. The previous equation shows that, as predictable, the confidence interval width becomes narrower as N increases. In this case, the Student's t-distribution approaches the standard normal distribution. In the limit situation – obviously hypothetical – in which N tends to infinity, there is no statistical uncertainty and the confidence interval converges towards $E[D(T)]$.

Case 2 is now considered. This is a special case of Case 1 with $N = 1$. Since only one single time-history $x(t)$ is available, the sample mean and the sample variance of the damage cannot be

computed as done before. A slightly different procedure is then proposed to construct the confidence interval. The main principle is to divide the time-history into N_B disjoint blocks of equal length, $T_B = T/N_B$, see Figure 8(b). This type of block subdivision has also been adopted in [45], though for a different purpose. For a fixed total duration T, the quantities N_B and T_B are inversely proportional.

After the block subdivision, the damage of the entire time-history $x(t)$, see Eq. (6), can be calculated by summing up the damage of all blocks:

$$D(T) \cong \sum_{i=1}^{N_B} D_{B,i}(T_B) = N_B \cdot \overline{D}_B(T_B) \tag{32}$$

where N_B is the number of blocks, $D_{B,i}(T_B)$, $i = 1,2,...N_B$ is the damage of each block and $\overline{D}_B(T_B) = N_B^{-1} \sum_{i=1}^{N_B} D_{B,i}(T_B)$ represents the sample mean of the damage values of all blocks. A minimum number of blocks $N_B \geq 2$ is required.

It has to be noted that the first equality in Eq. (32) is not exact. Indeed, since the separation into blocks discontinues the time-history at those points connecting two adjacent blocks, some fatigue cycles could be lost. More precisely, the block subdivision eliminates all the cycles formed by those peaks and valleys that, after subdivision, end up in different blocks. It may be presumed that this effect is less pronounced in a narrow-band process in which fatigue cycles are formed by the two nearest peak and valley. Accordingly, in theory, the sum of block damage values as in Eq. (32) would be slightly smaller than the damage of the whole continuous time-history in Eq. (6) [45]. This difference, however, is negligible if the number of cycles in each block is much greater than the number of blocks. For example, each block must have a minimum length T_B so to contain approximately 10^3 cycles, which is about the lower bound of high-cycle fatigue applications. This result means that N_B cannot increase indefinitely. The negligible effect of the block subdivision on the number of lost cycles will be confirmed by the simulation results presented in subsequent figures.

The damage values $D_{B,i}(T_B)$ have in common also the same variance. In fact, as the entire $x(t)$ is stationary, every time-history $x_i(t)$ in each block has the same statistical properties of $x(t)$.

Since all blocks also have the same length, the damages $D_{B,i}(T_B)$ form a set of random variables that follow the same probability distribution, with expected value $E[D_B(T_B)]$ and variance $\sigma^2_{D_B}$. Furthermore, as the blocks are disjoint (not overlapped), the random variables $D_{B,i}(T_B)$ are also independent.

Based on the assumption that the damage values of each block, $D_{B,i}(T_B)$, are independent and identically distributed, the variance σ^2_D of the damage of the whole time-history $x(t)$ can be written as:

$$\sigma^2_D = \mathrm{Var}\left[\sum_{i=1}^{N_B} D_{B,i}(T_B)\right] = N_B \cdot \sigma^2_{D_B} \tag{33}$$

where $\sigma^2_{D_B} = \mathrm{Var}(D_{B,i}(T_B))$ is the variance common to all blocks. And given that the variance σ^2_D must remain constant, the quantities $\sigma^2_{D_B}$ and N_B are inversely proportional, i.e. the shorter is the block length T_B, the higher the variance of the damage in each block.

The relationship in Eq. (33) involves the "true" (but unknown) variances; it can however be approximated as $\sigma^2_D \cong N_B \cdot \hat{\sigma}^2_{D_B}$, in which the block variance is replaced by its sample estimate $\hat{\sigma}^2_{D_B} = (N_B - 1)^{-1} \sum_{i=1}^{N_B} [D_{B,i}(T_B) - \overline{D}_B(T_B)]^2$.

Separation into blocks then produces N_B damage values $D_{B,i}(T_B)$ characterized by the sample mean $\overline{D}_B(T_B)$ and the sample variance $\hat{\sigma}^2_{D_B}$, which is exactly the same situation as Case 1. Therefore, in the same way as Eq. (31), it is now possible to establish a confidence interval that includes the expected damage of blocks, $E[D_B(T_B)]$. By following the mathematical steps described in Appendix B, the final confidence interval expression for $E[D(T)]$ when considering only one time-history $x(t)$ is:

$$D(T) - t_{dof,\beta/2} \cdot \hat{\sigma}_D \leq E[D(T)] \leq D(T) + t_{dof,\beta/2} \cdot \hat{\sigma}_D \tag{34}$$

where $t_{dof,\beta/2}$ is the quantile of Student's t-distribution with $dof = N_B - 1$ degrees of freedom, $D(T)$ is the fatigue damage of $x(t)$ and $\hat{\sigma}_D \cong \sqrt{N_B} \cdot \hat{\sigma}_{D_B}$ the sample variance of the damage computed, respectively, from Eq. (32) and (33). Note that, although the number of blocks does not appear directly in Eq. (34), it is used to compute $D(T)$ and $\hat{\sigma}_D$.

For large dof, the Student's t-distribution approaches a standard normal distribution. Therefore, when the number of blocks becomes large (for example, >30), approximating $t_{dof,\beta/2}$ with $z_{\beta/2}$ introduces an error of only a few percent (more exactly, from 6% for $N_B = 30$ down to 3% for $N_B = 30$), which is acceptable from an engineering standpoint.

The expression in Eq. (34) shows that, as N_B increases, the confidence interval width tends to become narrower because $t_{dof,\beta/2}$ diminishes towards the quantile $z_{\beta/2}$ of the standard normal variable. While for small N_B the difference is appreciable, for higher values (for example, for $N_B = 25$) the two quantiles, as already said, only differ of a few percentage points. However, the number of blocks N_B cannot increase indefinitely, as it must guarantee that the time-history in each block has a minimum number of fatigue cycles, as emphasized earlier.

There is, however, a substantial difference between Case 1 and Case 2. In the first case, the statistical uncertainty reduces if one has available a large number of time-histories; this circumstance, though, is not always achievable in practice where it may be difficult to collect a large number of time-histories. In the second case in which only one time-history is available, instead, the statistical uncertainty cannot be reduced by simply increasing the number of blocks.

8.2 Verification of the confidence interval expressions: numerical example

This example intends to evaluate the correctness of the previous confidence interval expressions; in simulations, it considers the Wirsching's formula of the output stress PSD in an offshore platform [43]:

$$S(f) = \frac{GH_s^{\varphi}\exp\left[-\dfrac{1050}{(2\pi f T_W)^4}\right]}{T_W^4(2\pi f)^5\left[\left(1-\dfrac{f^2}{f_n^2}\right)^2+\left(\dfrac{2\zeta f}{f_n}\right)^2\right]} \tag{35}$$

In this expression, G and φ are scaling factors, f_n = first resonance frequency (in Hz), H_s = significant wave height (in meters), T_W = dominant wave period (in seconds). Each sea state is characterized by a specific combination of H_s and T_W, which makes the shape of $S(f)$ change from narrow-band to bimodal. The parameter values φ, H_s, T_W depend on the sea state, whereas the others G, f_n, ζ do not. In this example, the following parameter values are chosen: $G = 5580$, $\varphi = 3.25$, $f_n = 0.286$ Hz, $\zeta = 0.02$. Besides, two different combinations of H_s, T_W are considered: the first one ($H_s = 0.76$ m, $T_W = 3.36$ s) yields a narrow-band PSD characterized by $\alpha_1 = 0.998$, $\alpha_2 = 0.992$, the second one ($H_s = 16.01$ m, $T_W = 17.3$ s) yields a wide-band (more precisely, bimodal) PSD with $\alpha_1 = 0.776$, $\alpha_2 = 0.506$. The two power spectra are compared in Figure 9; for simplicity, the zero-order moment is normalized to $\lambda_0 = 1$.

The formula in Eq. (35) is meant to represent an exact PSD, with no statistical variability. The corresponding expected damage $E[D(T)]$ can be computed by Eq. (9) for the narrow-band case, whereas for the wide-band case the TB method in Ref. [39] is used. It represents a sort of "reference" damage value that is used to verify the correctness of confidence interval expressions. Damage calculation assumes a S-N curve $s^k N_f = A$ with $A = 1$, $k = 3$. Like the expected damage, also the variance σ_D^2 computed from $S(f)$ by the method of Madsen et al. in Eq. (22) represents a "reference" value for the narrow-band case. In the wide-band case no mathematical formula exists to compute σ_D^2, therefore the "reference" value σ_D^2 was approximated by results of Monte-Carlo simulations.

It is useful to underline that the power spectral density $S(f)$ in Eq. (35) has a twofold role. On one hand, it is the power spectrum from which representative time-history realizations are simulated, as described below. On the other hand, it provides the expected damage $E[D(T)]$ and the variance σ_D^2 that, being "reference" values, allow the correctness of the confidence intervals to be checked (such

two "reference" values represent unknown population parameters that are not required when, in practice, one applies the concept of confidence interval).

Random stationary Gaussian time-histories $x_i(t)$, $i = 1,2,...N$ of equal time-length T are simulated directly from $S(f)$, either narrow-band or wide-band. The length T is selected as to give approximately $2 \cdot 10^4$ cycles. As done before, the time-histories are generated by using the Discrete Fourier Transform approach, with deterministic spectral amplitudes and random phases [37,38].

A maximum of $N = 20$ is chosen. For each different value of N, a new different set of time-histories is simulated, for a total of $1 + 2 + 3... + 19 + 20 = 210$ time-histories. The single time-history (for $N = 1$) is analyzed as per Case 1 and the multiple time-histories (for $N \geq 2$) are analyzed as per Case 2 described previously. The results are plotted in Figure 10 (narrow-band PSD) and Figure 11 (wide-band PSD) to show how the two confidence intervals actually work. The damage values shown in all figures are normalized to the expected damage.

On the other hand, it is necessary that a much larger set of time-histories is analyzed before conclusions can be made on the correctness of the confidence intervals in Eq. (31) and (34). To this end, the time-history simulation procedure just described was repeated a total of $2 \cdot 10^5$ times. Therefore, Figure 10 and Figure 11 only show one example out of a total of $2 \cdot 10^5$ similar results that form the entire dataset – for obvious reasons, it is not possible to show all the results in their entirety.

More precisely, Figure 10(a) and Figure 11(a) compare the expected damage to the 95% confidence interval in Eq. (31), as a function of the number of time-histories, N. The confidence interval is drawn around the mean damage $\overline{D}(T)$ of each set of time-histories. For any N, the expected damage always falls within the confidence interval. This result, though, cannot be generalized as – for what said above – Figure 10 and Figure 11 only show one example from a much larger set for which it is expected that only 5% of the time the expected damage would fall outside the confidence interval (this indeed corresponds to the definition of a 95% confidence interval).

It can be observed that the confidence interval becomes narrower as the number of time-history increases. This suggests the need to use as many time-histories as possible to get a narrow confidence interval. Of course, the interval would be larger if the confidence level $100(1-\beta)$ were higher.

Figure 10(b) and Figure 11(b) compare, instead, the expected damage $E[D(T)]$ to the 95% confidence interval in Eq. (34), as a function of the number of blocks, N_B. In both figures, the damage $D(T)$ computed by Eq. (32) apparently shows no scatter and looks even constant. This negligible scatter with N_B (of less than 1%) actually confirms how insignificant is the number of cycles being lost after subdividing the whole time-history into blocks (this occurs even for the wide-band process). This result then confirms the validity of Eq. (32).

For this particular example, the confidence interval encloses the expected damage all over the number of blocks considered. The figure also displays the confidence interval analogous to Eq. (34), but constructed with the "true" standard deviation, σ_{D}, of the damage of the random process, and computed by the Madsen et al. method directly from the "true" power spectrum $S(f)$.

It may be noticed that, as the number of blocks increases, the confidence interval constructed around the damage $D(T)$ converges to the confidence interval based on the "true" standard deviation. This result highlights, on one hand, the importance of considering as many blocks as possible to narrow the confidence interval, provided that each block is enough long to give a sufficient number of cycles. It also highlights, on the other hand, that the confidence interval width does not converge to zero as the number of blocks increases; but it approaches the scatter of the damage that characterizes the random process.

In this example, the expected damage $E[D(T)]$ is known and it was used to check the correctness of confidence interval expressions. By contrast, in practice the expected damage is never known. This implies that it is not known whether the damage $D(T)$ from one time-history does underestimate or overestimate the expected damage. Note, however, that a structure would be designed unsafely if the expected damage were underestimated. The safe region is only that in which

$D(T)$ is greater than $E[D(T)]$. Since $E[D(T)]$ is actually unknown, it is recommended to take the upper confidence limit as a lowest reference value to be used in structure design.

The examples in Figure 10 and Figure 11 show that the expected damage always falls within the confidence limits. It has, however, to be emphasized that both figures only refer to one single result out of a total of $2 \cdot 10^5$ similar ones. This means that if another simulation were performed, the expected damage could fall either inside or outside the confidence interval. The interpretation of a 95% confidence is that 5 out of 100 simulations would fall outside.

Therefore, a conclusion about the correctness of the confidence interval expressions can only be made by analyzing the whole set of $2 \cdot 10^5$ replicated samples and counting for each of them how many times the confidence interval encloses the expected damage. Virtually, this number should be equal to 95%.

Figure 12(a) and Figure 13(a) show a subset of 20 confidence intervals, for the case of $N = 20$ time-histories with about $2 \cdot 10^4$ cycles each (for better clarity, not all confidence intervals are shown). Note that few confidence intervals do not contain the expected damage, while the others do. The ratio between the number of confidence interval containing the expected damage to the total number of intervals provides an estimated confidence $100(1 - \hat{\beta})\% = 94.48\%$ for both the narrow-band and the wide-band PSD cases, which is almost coincident with the theoretical value.

The same argument also applies to the case of only one time-history (details in Figure 12(b)), for which the estimated confidence is $100(1 - \hat{\beta})\% = 94.49\%$ for the narrow-band PSD, whereas a value of 94.48% follows from the wide-band PSD.

9 CONCLUSIONS

The paper investigated the variability of the fatigue damage in stationary Gaussian random loadings that is caused by the inherent randomness of the load itself. Explicit formulas from the literature (Mark and Crandall, Bendat, Madsen et al. and Low) were reviewed and compared with Monte Carlo

simulation results in the both time- and the frequency-domain. A large sample of time-histories were simulated from several types types of power spectral density (linear oscillator system, unimodal, Pierson-Moskowitz, JONSWAP). The sample statistics (mean, variance, coefficient of variation) were determined for the fatigue damage in both time- and frequency domain, and then compared to the estimations provided by the explicit formulas. A perfect agreement resulted, at least for the specific power spectrum type for which each of the formulas applies. In fact, while some methods (Mark and Crandall, Bendat) are restricted to the linear oscillator and to either odd or even values of the S-N slope, the other two (Madsen et al. and Low) are far more general, with no restriction on the particular shape of narrow-band power spectrum or on the S-N slope value. Results also showed that the scatter around the expected damage reduces as the time-history length increases. It was also observed how the CoV is a smooth monotonic function of bandwidth parameters α_1 and α_2, a feature that permitted a best-fitting expression to be proposed and then calibrated on the results of each power spectral density considered individually, as well as on the results of all power spectra merged together. Not only are the proposed expressions rather simple and easy to be used in practice, but they also agree with time-domain simulation results.

In its second part, the paper addressed the issue of estimating the statistical variability of the fatigue damage in the situation in which it is computed from only few time-histories (Case 1) or from only one (Case 2). For each of the two cases, the paper derived a confidence interval expression to enclose the (unknown) expected fatigue damage. An example confirmed the correctness of both confidence interval expressions. The example considered the stress power spectral density in an offshore platform, as proposed by Wirsching et al. (1976). Sample statistics (mean and variance) of the damage from simulated time-histories were used to construct the confidence interval, which was then compared to the expected damage computed directly from the power spectrum (it represents the reference value needed by the analysis to check whether the confidence interval correctly encloses the expected damage, for a prescribed confidence). By replicating the analysis a large number of times ($2 \cdot 10^5$) and counting how many times the confidence interval encloses the expected damage,

the analysis returned an estimated confidence of nearly 94.48% in either cases examined, a value almost coincident with the theoretical one 95% previously assumed. This confirmed the validity of the proposed approach.

APPENDIX A

The Pierson-Moskowitz spectrum is described by the following equation [42,46]:

$$S(f) = \frac{\alpha g^2}{(2\pi f)^4}\exp\left(-\frac{5}{4}\left(\frac{f_p}{f}\right)^4\right) \tag{36}$$

where $f_p = {}^1/_{T_W}$ is the peak frequency and T_W the peak period (dominant wave period) of the spectrum, $\alpha \approx 5.061\left(H_s^2/T_p^4\right)$, H_s the significant wave height, and g is the gravity constant.

The JONSWAP spectrum is a generalization of the P-M spectrum [46,47]:

$$S(f) = \frac{\alpha g^2}{(2\pi f)^4}\exp\left(-\frac{5}{4}\left(\frac{f_p}{f}\right)^4 + \log(\kappa)\exp\left(\frac{-\left(\frac{f}{f_p}-1\right)^2}{2\sigma^2}\right)\right) \tag{37}$$

where $\alpha \approx 5.061\left(H_s^2/T_W^4\right)[1 - 0.287\ln(\kappa)]$ is the normalization factor and $\sigma = 0.07$ if $f < f_p$ and $\sigma = 0.09$ if $f \geq f_p$, and it is often $\kappa = 3.3$.

APPENDIX B

This section explains how Eq. (34) is derived. The starting point is the confidence interval for the expected damage of a single block of time length T_B:

$$\overline{D}_B(T_B) - \frac{t_{dof,\beta/2} \cdot \hat{\sigma}_{D_B}}{\sqrt{N_B}} \leq E[D_B(T_B)] \leq \overline{D}_B(T_B) + \frac{t_{dof,\beta/2} \cdot \hat{\sigma}_{D_B}}{\sqrt{N_\mathrm{B}}} \tag{38}$$

Multiplying this expression by the number of blocks N_B yields:

$$N_B\left(\overline{D}_B(T_B) - \frac{t_{dof,\beta/2} \cdot \hat{\sigma}_{D_B}}{\sqrt{N_B}}\right) \leq N_B \cdot E[D_B(T_B)] \leq N_B\left(\overline{D}_B(T_B) + \frac{t_{dof,\beta/2} \cdot \hat{\sigma}_{D_B}}{\sqrt{N_B}}\right) \tag{39}$$

As N_B is deterministic, the expected value of Eq. (32) yields:

$$E[D(T)] = E\left[\sum_{i=1}^{N_B} D_{B,i}(T_B)\right] = N_B \cdot E[D_B(T_B)\,] \tag{40}$$

This result can also be obtained from Eq. (9) by noting that $E[D_B(T_B)\,] = \left(T_B/T\right) \cdot E[D(T)]$. Substituting into Eq. (39) and considering the approximation $\hat{\sigma}_D \cong \sqrt{N_B} \cdot \hat{\sigma}_{D_B}$ of Eq. (33), gives:

$$D(T) - t_{dof,\beta/2} \cdot \hat{\sigma}_D \leq E[D(T)] \leq D(T) + t_{dof,\beta/2} \cdot \hat{\sigma}_D \tag{41}$$

which coincides with the confidence interval expression also reported in Eq. (34).

REFERENCES

1 Dirlik T. Application of computers in fatigue analysis. Ph.D. thesis. UK: University of Warwick; 1985.

2 Larsen CE, Lutes LD. Predicting the fatigue life of offshore structures by the single-moment method. Probab Eng Mech 1991;6(2):96–108. https://doi.org/10.1016/0266-8920(91)90023-W

3 Benasciutti D, Tovo R. Comparison of spectral methods for fatigue analysis of broad-band Gaussian random processes. Probab Eng Mech 2006;21(4):287–299. doi: 10.1016/j.probengmech.2005.10.003

4 Benasciutti D, Tovo R. Frequency-based fatigue analysis of non-stationary switching random loads. Fatigue Fract Eng Mater Struct 2010;30(11):1016–1029. https://doi.org/10.1111/j.1460-2695.2007.01171.x

5 Benasciutti D, Cristofori A. A frequency-domain formulation of MCE method for multi-axial random loadings. Fatigue Fract Eng Mater Struct 2008;31(11):937–948. https://doi.org/10.1111/j.1460-2695.2008.01283.x

6 Niesłony A, Böhm M. Frequency-domain fatigue life estimation with mean stress correction. Int J fatigue 2016;91(2):373–381. https://doi.org/10.1016/j.ijfatigue.2016.02.031

7 Benasciutti D. Braccesi C, Cianetti F, Cristofori A, Tovo R. Fatigue damage assessment in wide-band uniaxial random loadings by PSD decomposition: outcomes from recent research. Int J Fatigue 2016;91(1):248–250. https://doi.org/10.1016/j.ijfatigue.2016.06.011

8 Mršnik M, Slavič J, Boltežar M. Vibration fatigue using modal decomposition. Mech Syst Signal Process 2018;98:548–556. https://doi.org/10.1016/j.ymssp.2017.03.052

9 Benasciutti D, Tovo R. Frequency-based analysis of random fatigue loads: Models, hypotheses, reality. Materialwiss Werkstofftech 2018;49(3):345-367. https://doi.org/10.1002/mawe.201700190

10 Niesłony A, Böhm M, Owsiński R. Formulation of multiaxial fatigue failure criteria for spectral method. Int J fatigue 2020;135:105519. https://doi.org/10.1016/j.ijfatigue.2020.105519

11 Capponi L., Slavič J, Rossi G, Boltežar M. Thermoelasticity-based modal damage identification. Int J Fatigue 2020;137: 105661. https://doi.org/10.1016/j.ijfatigue.2020.105661

12 Marques JME, Benasciutti D, Tovo R. Variance of fatigue damage in stationary random loadings: comparison between time- and frequency-domain results. Proc Struct Integrity 2019;24:398-07. https://doi.org/10.1016/j.prostr.2020.02.037.

13 Mark WD. The inherent variation in fatigue damage resulting from random vibration. Ph.D. Thesis, Department of Mechanical Engineering, M.I.T.; 1961.

14 Crandall SH, Mark WD, Khabbaz GR. The variance in Palmgren-Miner damage due to random vibration. In: Proceedings of the 4th US national congress of applied mechanics, vol. 1; 1962. p. 119–26.

15 Bendat JS. Probability functions for random responses: Prediction of peaks, fatigue damage, and catastrophic failures. NASA-CR-33; 1964.

16 Madsen HO, Krenk S, Lind NC. Methods of structural safety. Englewood Cliffs: Prentice-Hall; 1986.

17 Low YM. Variance of the fatigue damage due to a Gaussian narrowband process. Struct Saf 2012;34(1):381–9. https://doi.org/10.1016/j.strusafe.2011.09.001.

18 Lutes LD, Sarkani S. Random vibrations: analysis of structural and mechanical systems. Elsevier; 2004.

19 Bendat JS, Piersol AG. Random data: Analysis and measurement procedure. Hoboken: John Wiley & Sons, Inc.; 2010.

20 Longuet-Higgins MS. Statistical properties of wave groups in a random sea state. Philos. Trans. R. Soc. Lond. Ser. A-Math. 1984;312(1521):219-250. https://doi.org/10.1098/rsta.1984.0061

21 Rychlik I. Five lectures on reliability applications of Rice's formula for the intensity of level crossings. In: Jendo S, Dolinski K, editors. Course on Reliability-Based Design and Optimisation, Warsaw: Institute of Fundamental Technological Research; 2003, p. 241–323

22 Vanmarcke EH. Properties of spectral moments with applications to random vibration. J Eng mech Div-ASCE 1972;98(EM2):425-446. https://doi.org/10.1115/1.3423521

23 ISO/DIS 12107:2017 Metallic materials – Fatigue testing – Statistical planning and analysis of data.

24 Fatemi A, Yang L. Cumulative fatigue damage and life prediction theories: a survey of the state of the art for homogeneous materials. Int J Fatigue 1998;20(1):9–34. https://doi.org/10.1016/S0142-1123(97)00081-9

25 Sonsino CM. Fatigue testing under variable amplitude loading. Int J Fatigue 2007;29(6):1080–9. https://doi.org/10.1016/j.ijfatigue.2006.10.011

26 Hobbacher A. Recommendations for fatigue design of welded joints and components. IIW document IIW-2259-15; 2016.

27 Dowling NE. Estimation and correlation of fatigue lives for random loading. Int J Fatigue 1988;10(3):179-185. https://doi.org/10.1016/0142-1123(88)90060-6.

28 Sonsino CM. Course of SN-curves especially in the high-cycle fatigue regime with regard to component design and safety. Int J Fatigue 2007;29(12):2246-2258. https://doi.org/10.1016/j.ijfatigue.2006.11.015

29 Miles JW. On structural fatigue under random loading. J Aeron Sci 1954;21(11):753–62. https://doi.org/10.2514/8.3199

30 Rychlik I. On the 'narrow-band' approximation for expected fatigue damage. Probab Eng Mech 1993;8(1):1–4. https://doi.org/10.1016/0266-8920(93)90024-P

31 Krenk S, Madsen PH. Stochastic response analysis. In: Thoft-Christensen P, editor. Reliability theory and its application in structural and soil mechanics. NATO Advanced Study Institute Series, Springer-Verlag; 1983, p. 103–172.

32 Parzen E. Stochastic processes. Oakland: Holden-Day; 1962.

33 Rice SO. Mathematical analysis of random noise. Bell Syst Tech J 1944;23:282–32. https://doi.org/10.1002/j.1538-7305.1945.tb00453.x.

34 Low YM. Uncertainty of the fatigue damage arising from a stochastic process with multiple frequency modes. Probab Eng Mech 2014;36:8–18. https://doi.org/10.1016/j.probengmech.2014.02.001

35 Marques JME, Benasciutti D. More on variance of fatigue damage in non-Gaussian random loadings – effect of skewness and kurtosis. Proc Struct Integrity 2020; 25: 101-111. https://doi.org/10.1016/j.prostr.2020.04.014

36 Bengtsson A, Bogsjö K, Rychlik I. Uncertainty of estimated rainflow damage for random loads. Mar Struct 2009;22(2):261–274. https://doi.org/10.1016/j.marstruc.2008.05.001

37 Smallwood DO, Paez TL. A frequency domain method for the generation of partially coherent normal stationary time domain signals. Shock Vib 1993;1(1):45-53. https://doi.org/10.3233/SAV-1993-1106

38 Wirsching PH, Paez TL, Ortiz K. Random vibrations: Theory and practice. New York: John Wiley & Sons; 1995.

39 Benasciutti D, Tovo R. Spectral methods for lifetime prediction under wide-band stationary random processes. Int J Fatigue 2005;27(8):867–77. https://doi.org/10.1016/j.ijfatigue.2004.10.007.

40 Dodds CJ, Robson JD. The description of road surface roughness. J Sound Vib 1973;31(2):175–83. https://doi.org/10.1016/S0022-460X(73)80373-6.

41 Holmes JD. Wind loading of structures. 3rd ed. Boca Raton: Taylor & Francis Group; 2015.

42 Pierson Jr. WJ, Moskowitz L. A proposed spectral form for fully developed wind seas based on the similarity theory of S. A. Kitaigorodskii. J Geophys Res 1964;69(24):5181–90. https://doi.org/10.1029/JZ069i024p05181.

43 Wirsching PH, Preasthofer PH. Preliminary dynamic assessment of deepwater platforms. J Struct Division ASCE 1976;102(7):1447-62.

44 Montgomery DC, Runger GC. Applied statistics and probability for engineers. 6th ed. Hoboken, NJ, USA: John Wiley & Sons; 2014.

45 Costa RC, Sagrilo LVS. Statistical uncertainty analysis in time-domain fatigue assessment of steel risers. J Offshore Mech Arct Eng 2018;140(3):031701-1–10. https://doi.org/10.1115/1.4038583

46 Bengtsson A, Rychlik I. Uncertainty in fatigue life prediction of structures subject to Gaussian loads. Probab Eng Mech 2009;24(2):224–235. https://doi.org/10.1016/j.probengmech.2008.06.004

47 Hasselmann K, Barnett TP, Bouws E, Carlson H, Cartwright DE, Enke K, Ewing JA, Gienapp H, Hasselmann DE, Kruseman P, Meerburg A, Müller P, Olbers DJ, Richter K, Sell W, Walden H. Measurements of wind-wave growth and swell decay during the joint North Sea wave project (JONSWAP). Deutsches Hydrographischen Zeitschrift 1973;A12:1–95.

TABLES

Table 1. Best-fitting coefficients of Eq. (28) for each type of PSD, along with the fitting error e from Eq. (29).

PSD type	c_1	c_2	c_3	c_4	e
Linear oscillator	0.148	0.589	5.57	0.459	0.012
Unimodal	0.241	0.583	19.3	0.253	0.006
JONSWAP	0.237	0.590	10.3	0.238	0.003
Pierson-Moskowitz	0.223	0.594	22.4	0.319	0.002
All spectra	0.195	0.593	13.4	0.389	0.060

FIGURES

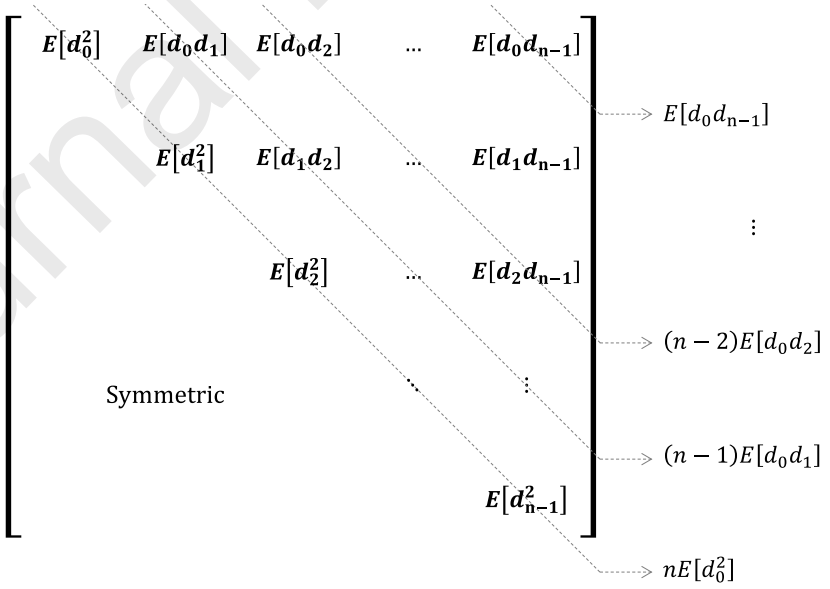

Figure 1. The double summation in Eq. (11) as an $n \times n$ matrix and the sum of elements in any diagonal.

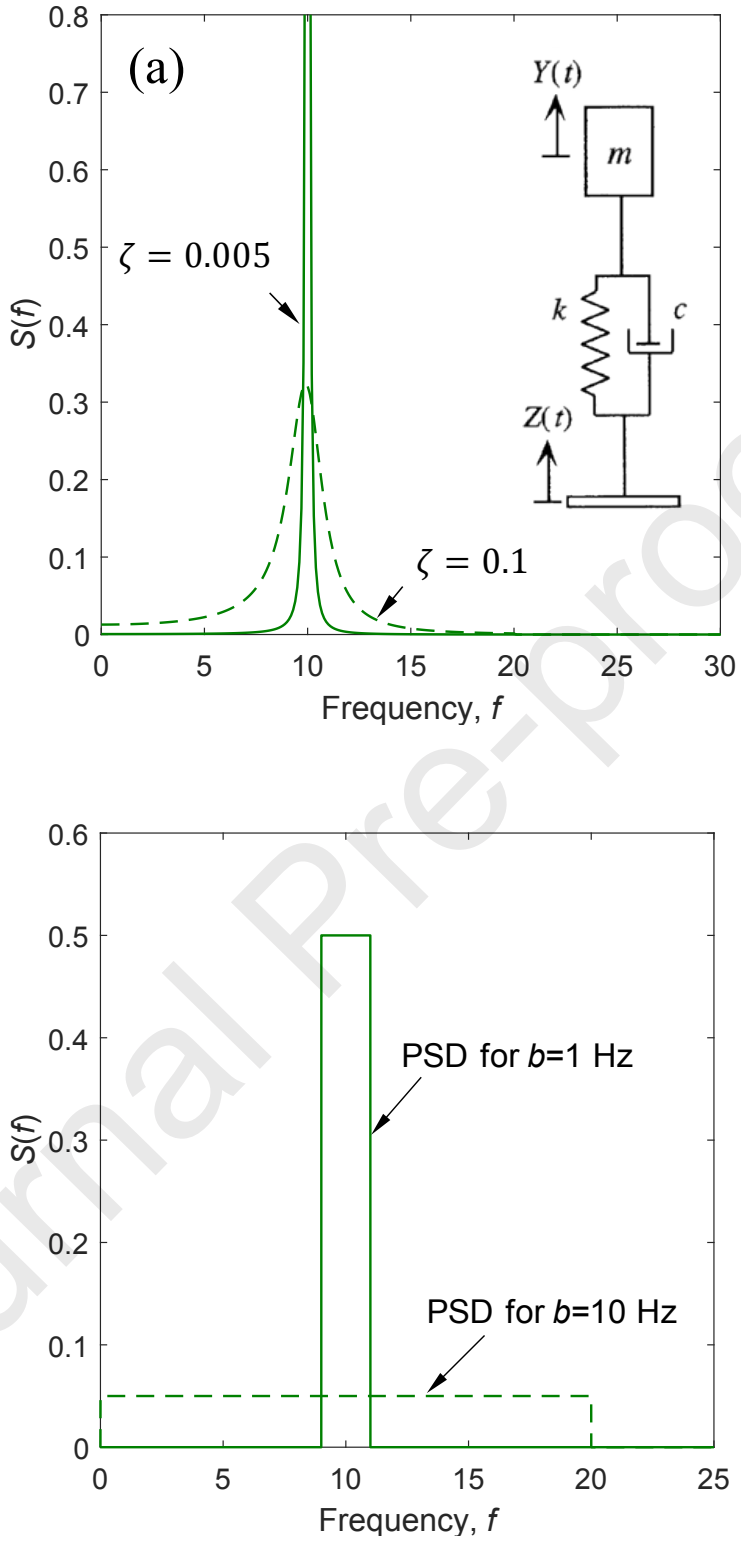

Figure 2. PSDs considered in numerical simulations: (a) linear oscillator system (for two limit values of damping), (b) ideal unimodal process (the dashed and the continuous line show the PSD with the narrowest and the widest half-spectral bandwidth).

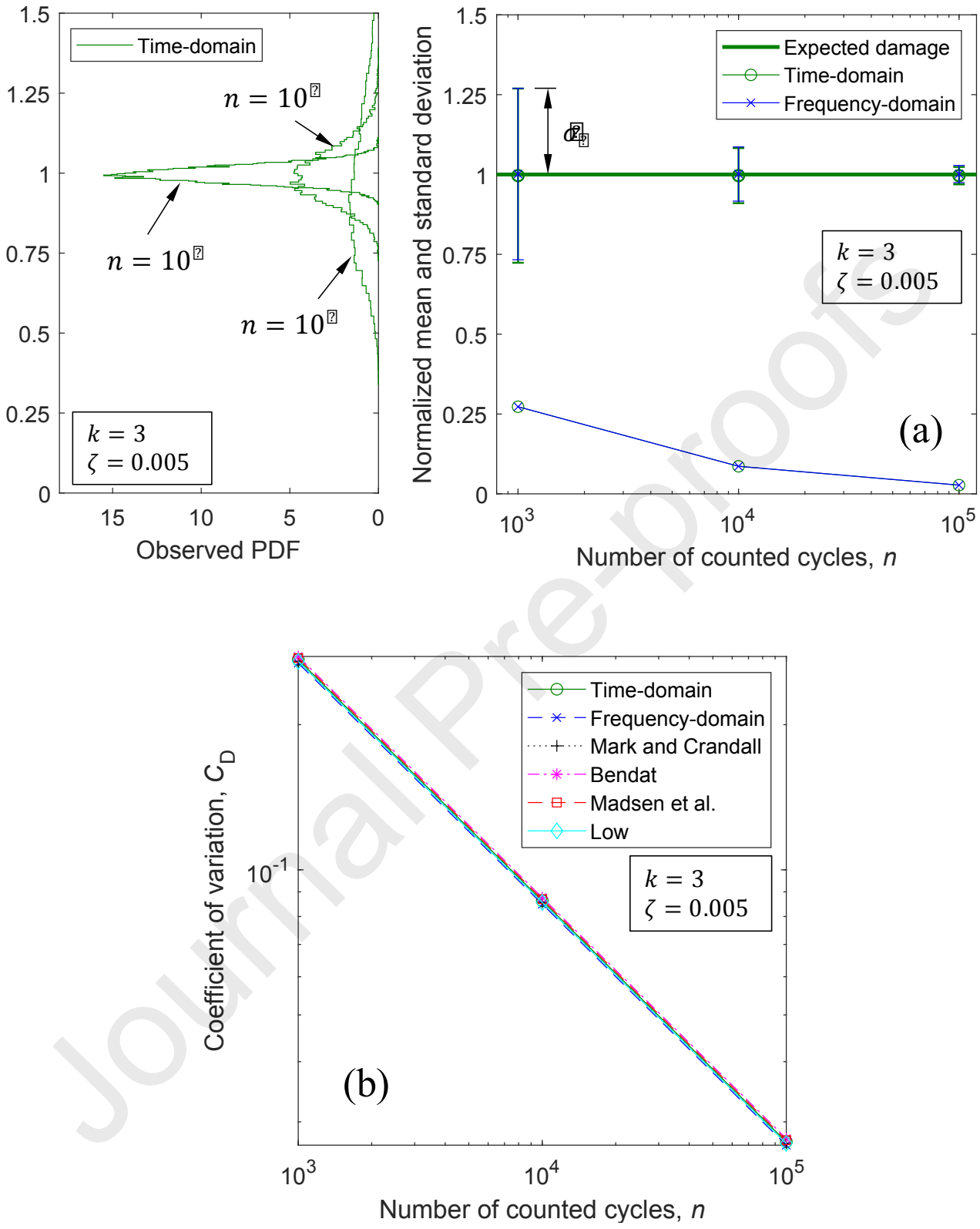

Figure 3. Simulation results for the linear oscillator system as function of the number of counted cycles (damping $\zeta = 0.005$, inverse slope $k = 3$): (a) sample mean and sample standard deviation of the damage (both normalized to the expected damage). The left box displays the observed probability distributions; (b) CoV of the damage.

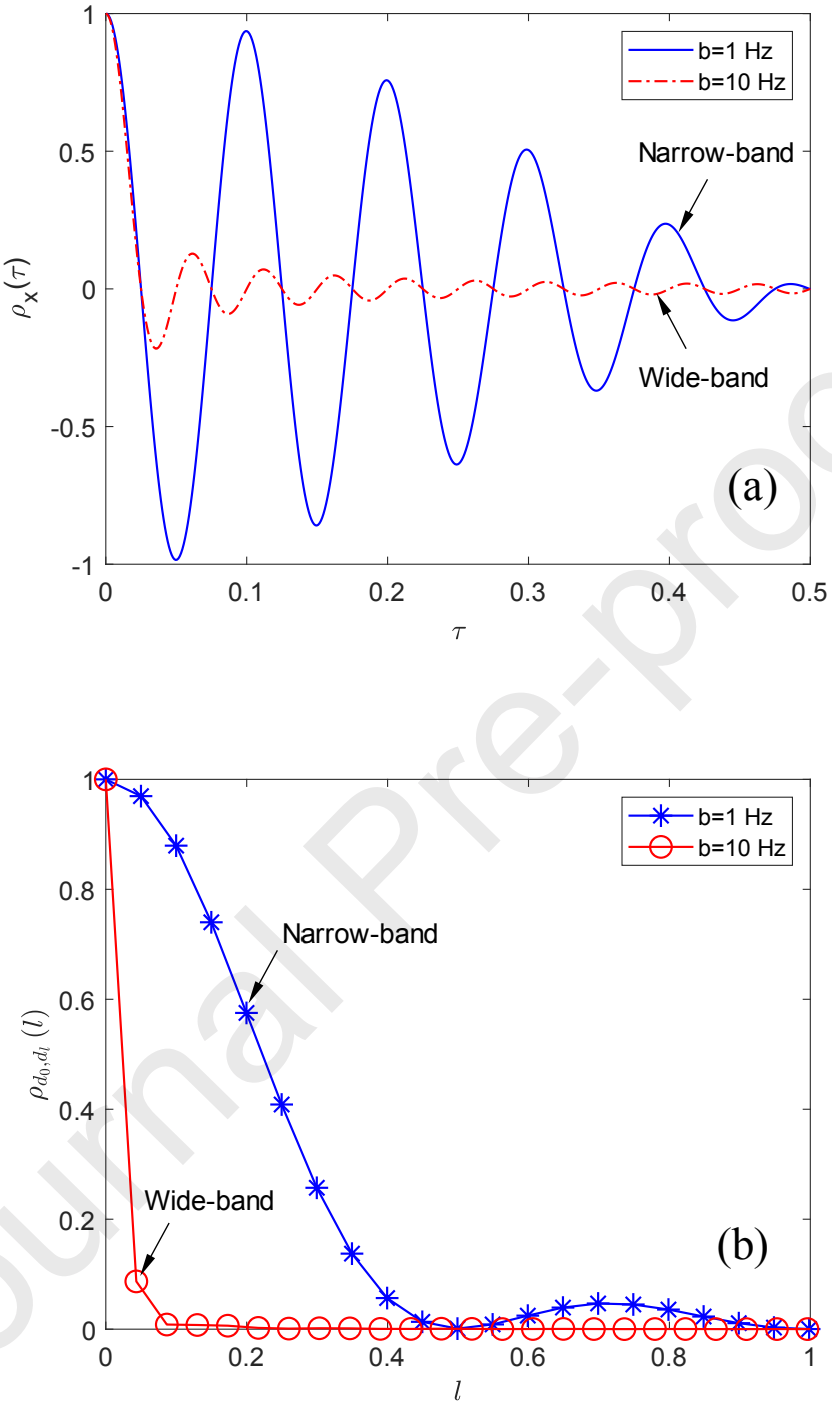

Figure 4. Comparison between the most narrow-band and most wide-band ideal unimodal process. Autocorrelation coefficient function of (a) the process and (b) the half-cycles damage.

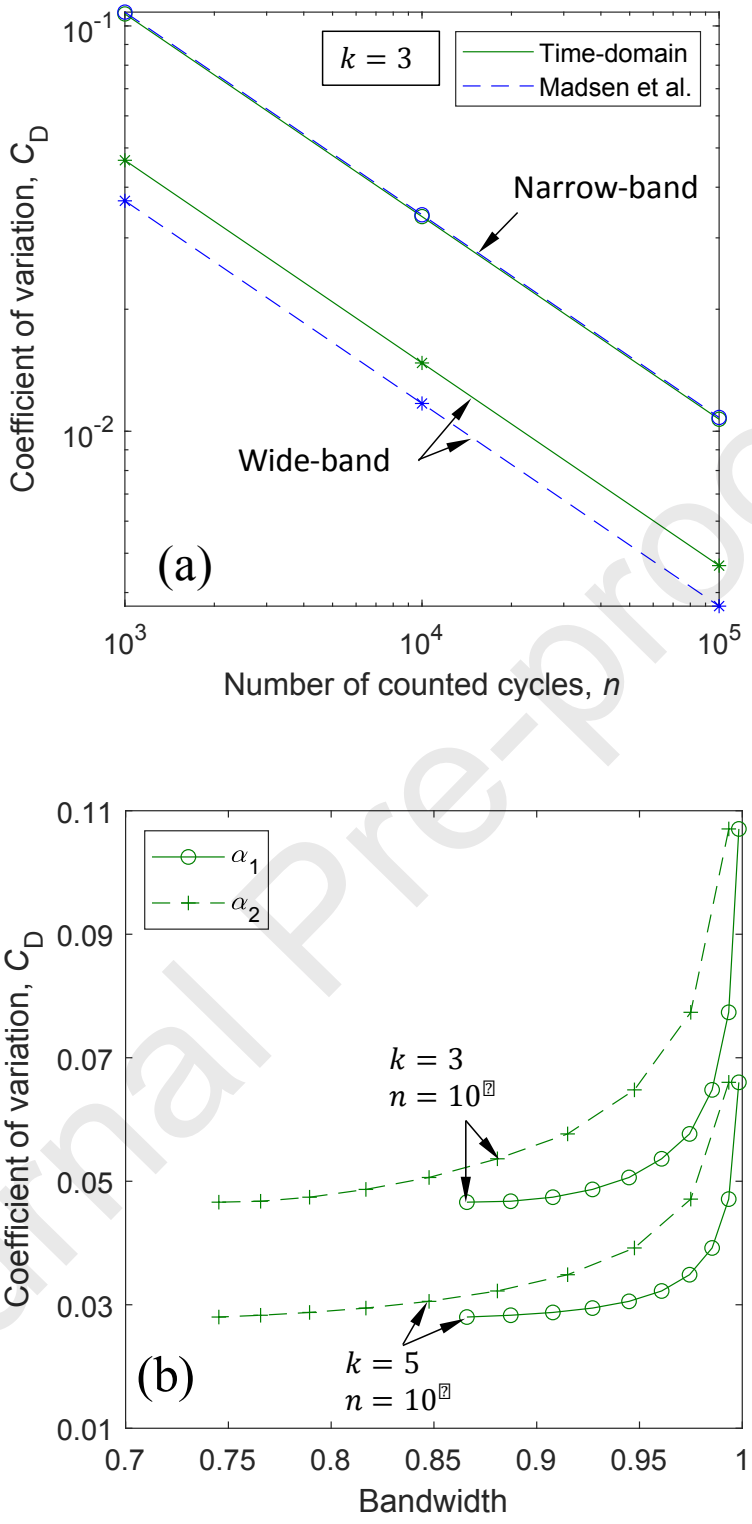

Figure 5. Ideal unimodal process: (a) CoV versus the number of cycles (for $k = 3$); (b) CoV versus α_1 and α_2, for two combinations of number of cycles and inverse slope k.

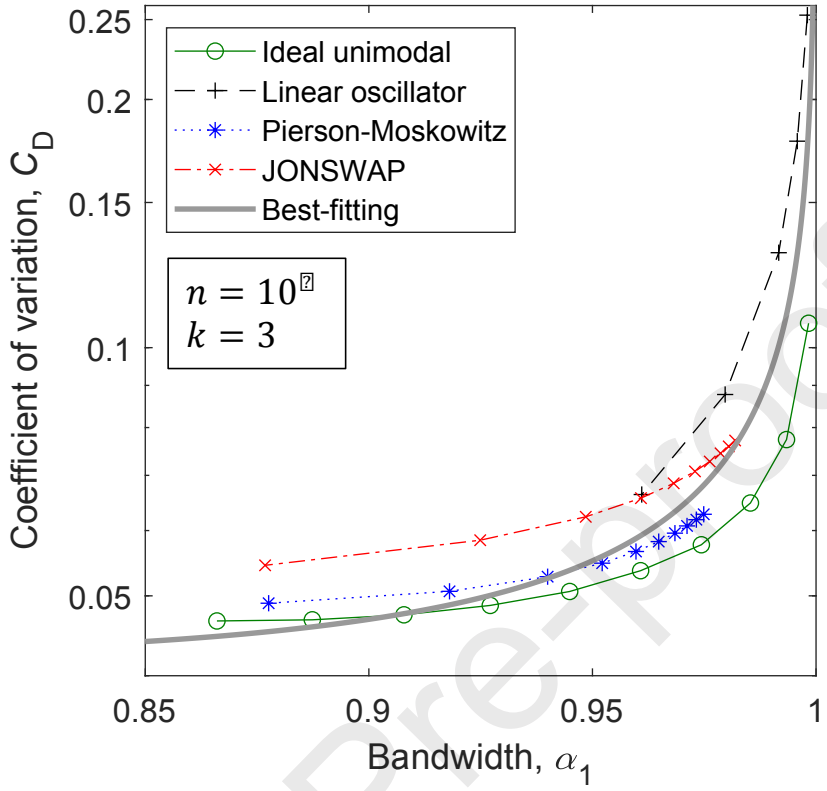

Figure 6. Comparison of the CoV for different PSDs, as a function of the bandwidth parameter α_1 (for $k = 3$ and 10^3 cycles). The continuous curve represents the best-fitted line.

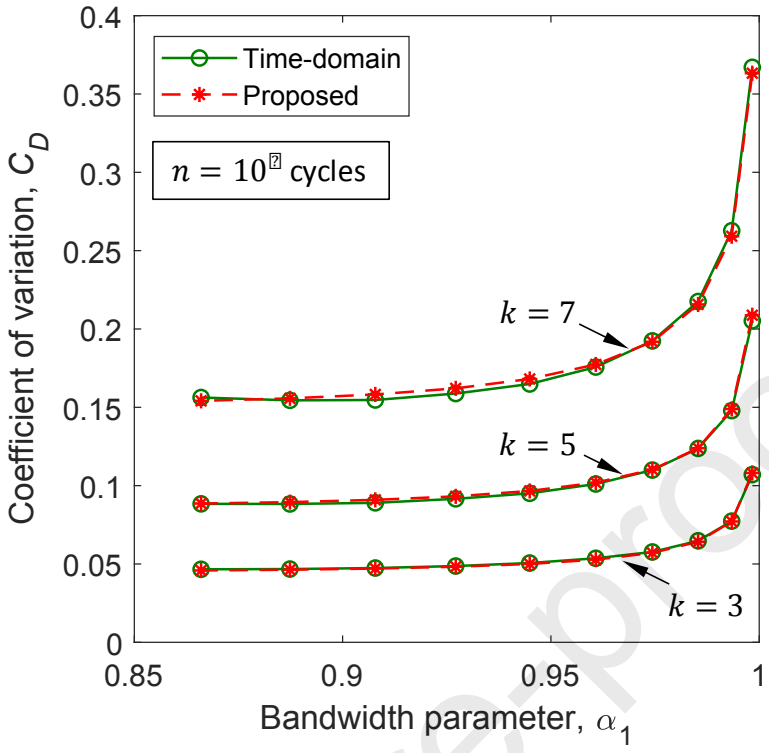

Figure 7. Ideal unimodal process: CoV versus α_1 (for 10^3 cycles). Comparison between the proposed best-fitting expression and the time-domain simulation results.

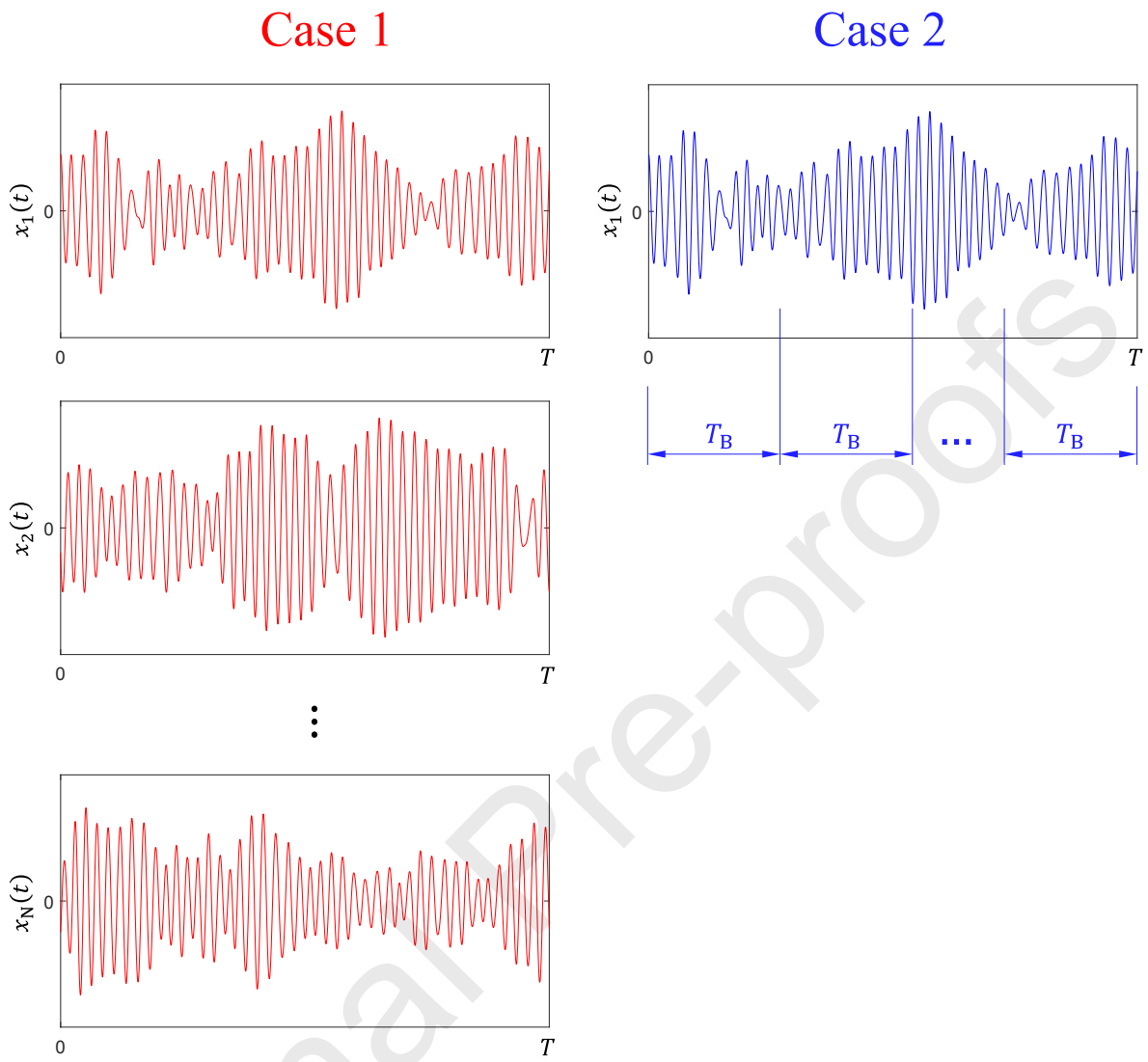

Figure 8. Two cases analyzed: (a) Case 1: two or more time-histories are available (the figure shows an example with N time-histories); (b) Case 1: only one time-history is available.

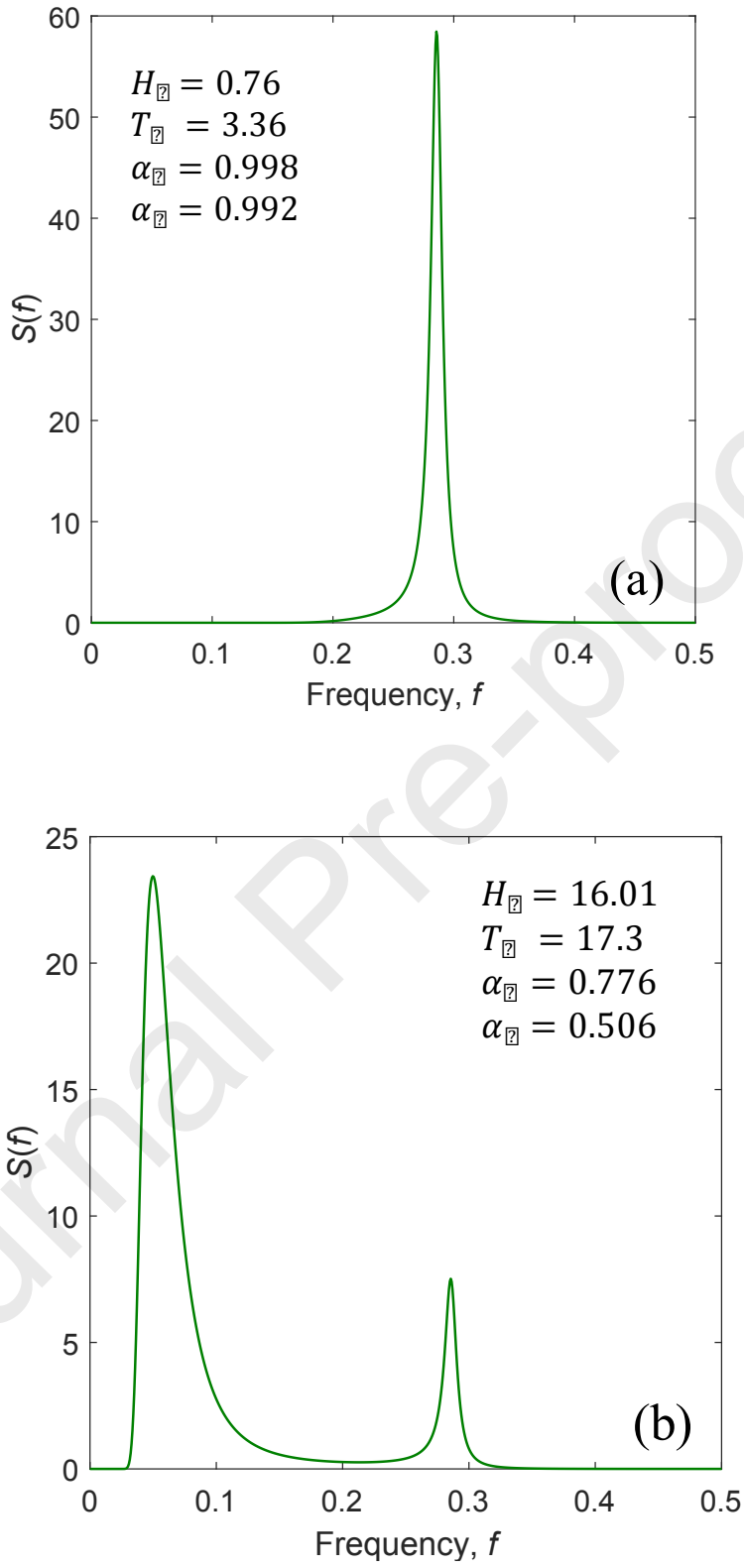

Figure 9. The two types of Wirsching's stress PSD used in numerical simulations: (a) narrow-band, (b) wide-bnad.

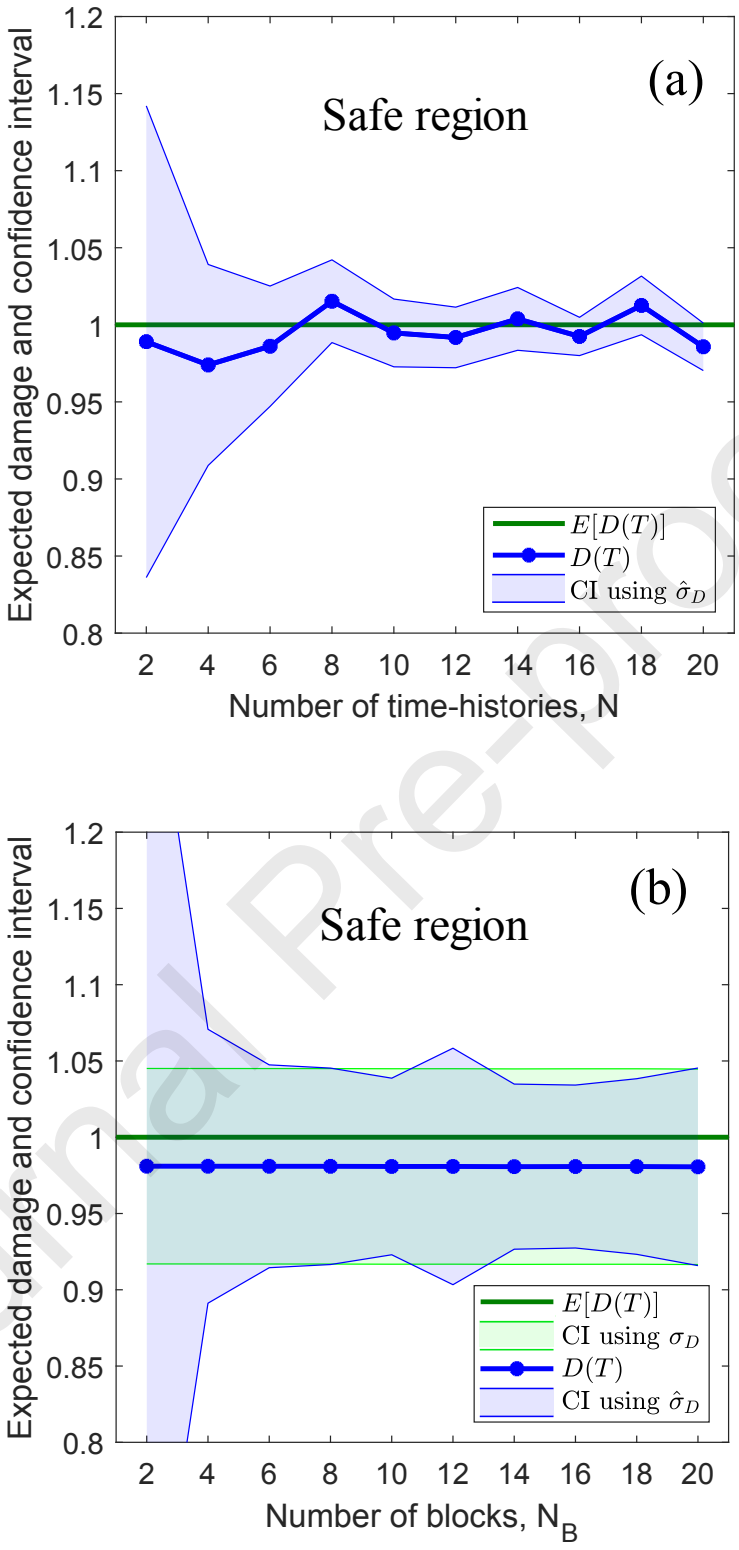

Figure 10. Confidence interval for Case 1 and Case 2, versus (a) the number of time-histories and (b) the number of blocks in one time-history. Results refer to the narrow-band PSD.

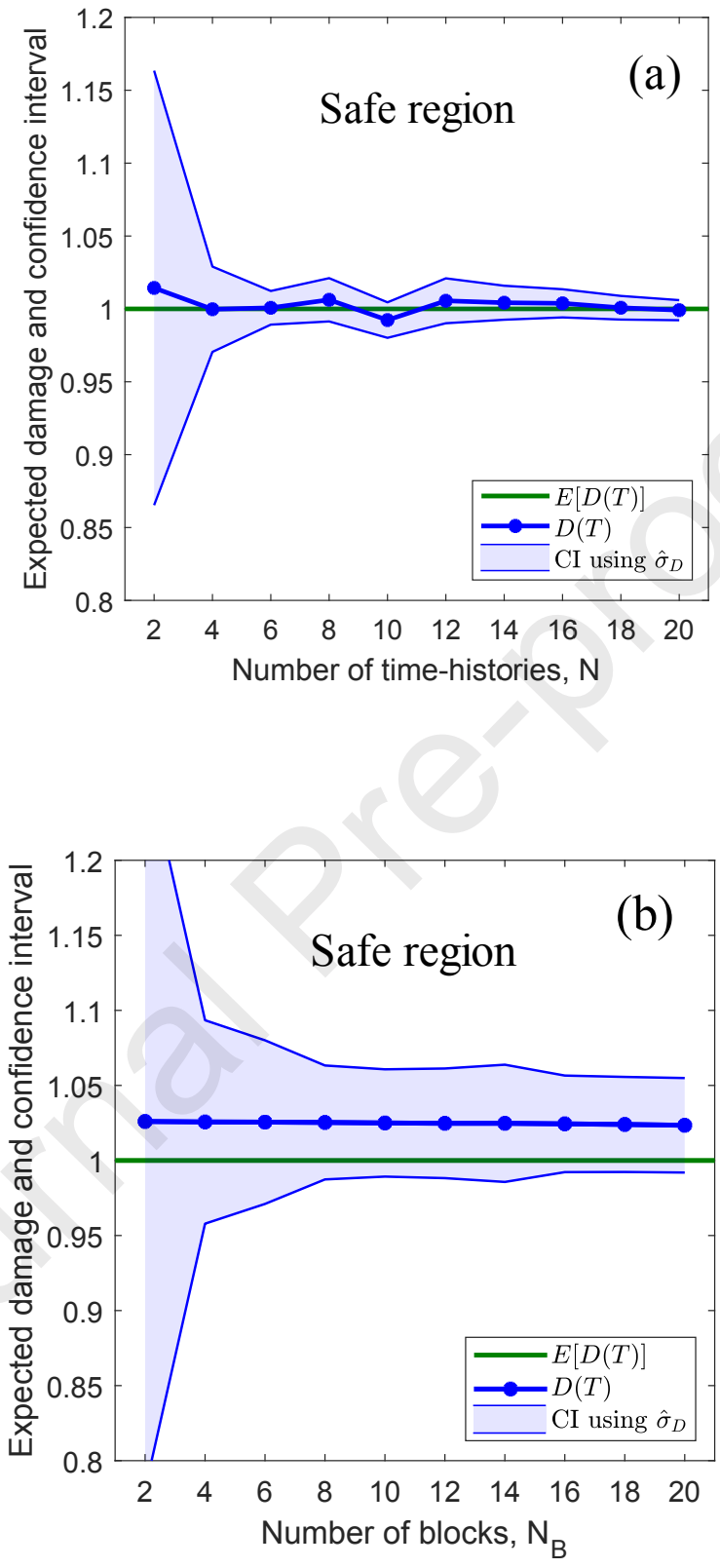

Figure 11. Confidence interval for Case 1 and Case 2, versus (a) the number of time-histories and (b) the number of blocks in one time-history. Results refer to the wide-band PSD.

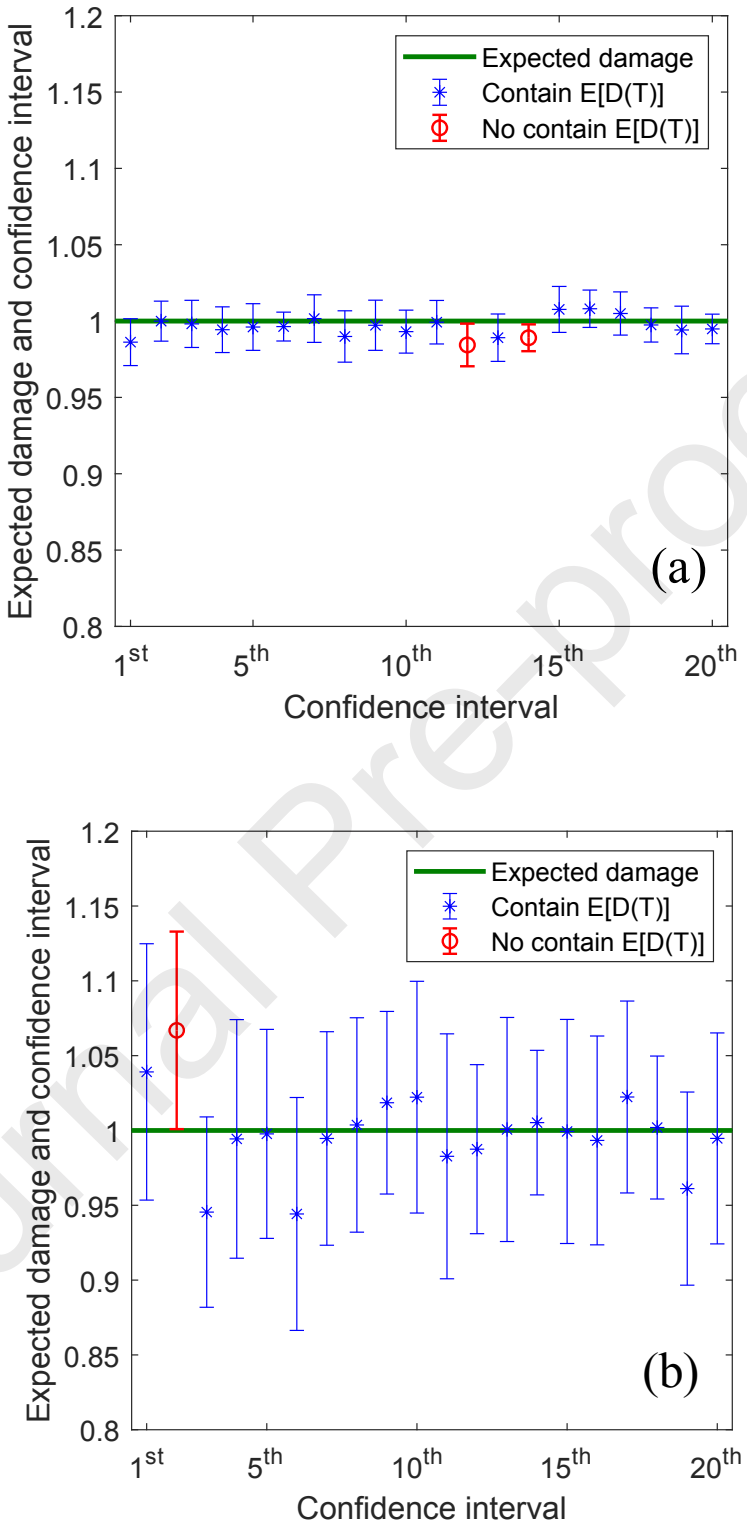

Figure 12. Check of confidence intervals using (a) $N = 20$ time-histories and (b) one time-history divided into $N_B = 20$ blocks. Results refer to the narrow-band PSD.

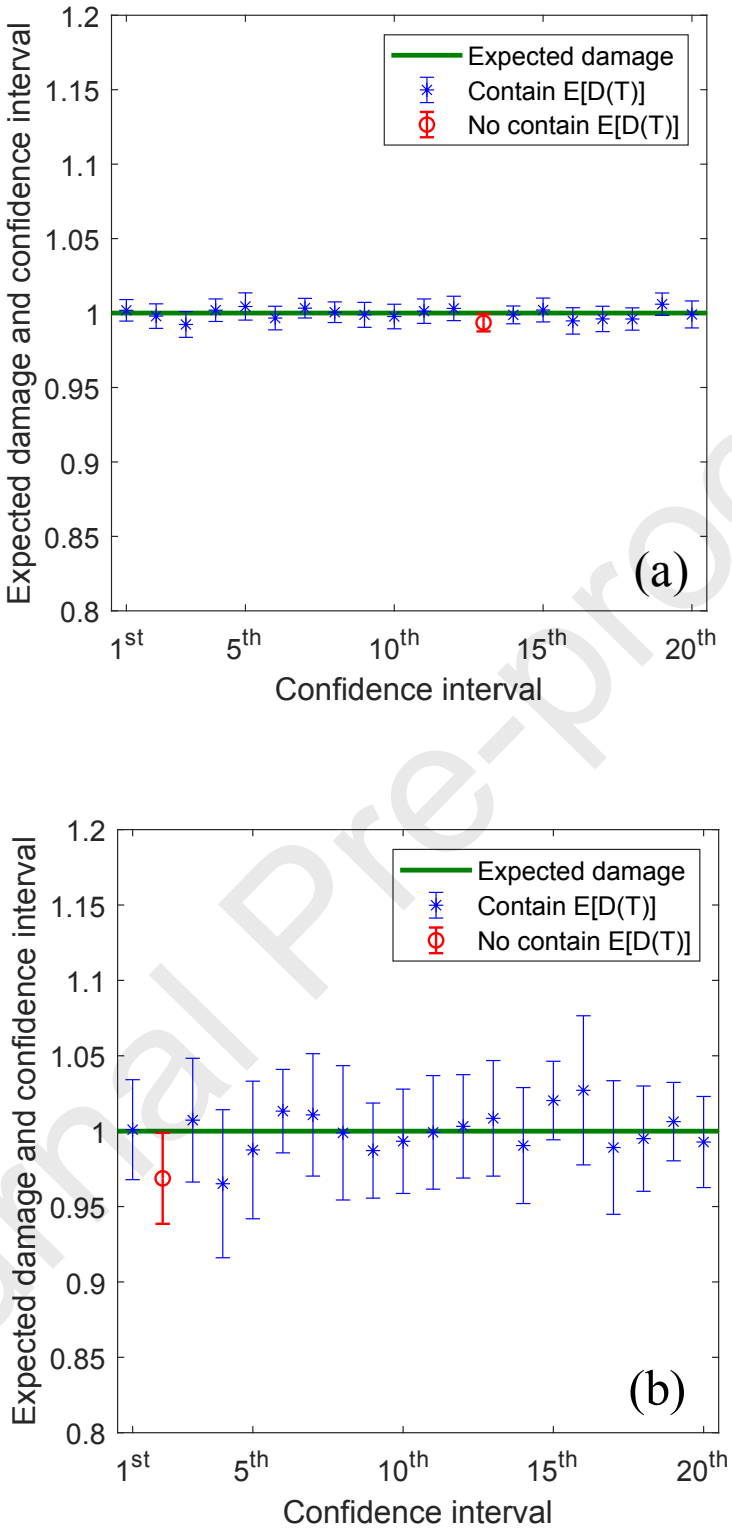

Figure 13. Check of confidence intervals using (a) $N = 20$ time-histories and (b) one time-history divided into $N_B = 20$ blocks. Results refer to the wide-band PSD.

Highlights:

- The variability of the fatigue damage in stationary Gaussian random loadings
- Review of existing methods to estimate the variability of the fatigue damage
- Best-fitting expressions to relate the variability of the fatigue damage to bandwidth parameters
- Confidence intervals for the expected damage from few time-histories

Declaration of interests

☒ The authors declare that they have no known competing financial interests or personal relationships that could have appeared to influence the work reported in this paper.

☐The authors declare the following financial interests/personal relationships which may be considered as potential competing interests: